AGU PUBLICATIONS

Geochemistry, Geophysics, Geosystems

RESEARCH ARTICLE

10.1002/2016GC006449

Key Points:
- Brucite-carbonate chimneys were found in a serpentinite-hosted seep system, Shinkai Seep Field in the southern Mariana forearc at ~5700 m deep
- The chimneys are subdivided into three types (I–III) in terms of appearances, vent activity, mineral composition, textures, and faunal communities
- Some characteristics of the SSF chimneys are different from previously reported chimneys at serpentinite-hosted vent/seep fields

Supporting Information:
- Supporting Information S1
- Movie S1

Correspondence to:
T. Okumura,
oktomy@kyudai.jp

Citation:
Okumura, T., et al. (2016), Brucite chimney formation and carbonate alteration at the Shinkai Seep Field, a serpentinite-hosted vent system in the southern Mariana forearc, *Geochem. Geophys. Geosyst.*, *17*, doi:10.1002/2016GC006449.

Received 24 MAY 2016
Accepted 7 SEP 2016
Accepted article online 10 SEP 2016

Brucite chimney formation and carbonate alteration at the Shinkai Seep Field, a serpentinite-hosted vent system in the southern Mariana forearc

T. Okumura[1], Y. Ohara[1,2], R. J. Stern[3], T. Yamanaka[4], Y. Onishi[4], H. Watanabe[5], C. Chen[1], S. H. Bloomer[6], I. Pujana[3], S. Sakai[7], T. Ishii[8], and K. Takai[1]

[1]Department of Subsurface Geobiological Analysis and Research (D-SUGAR), Japan Agency for Marine-Earth Science and Technology, Yokosuka, Japan, [2]Hydrographic and Oceanographic Department of Japan, Tokyo, Japan, [3]Geosciences Department, University of Texas at Dallas, Richardson, Texas, USA, [4]Graduate School of Natural Science and Technology, Okayama University, Okayama, Japan, [5]Marine Biodiversity Research Program, Japan Agency for Marine-Earth Science and Technology, Yokosuka, Japan, [6]Oregon State University, Corvallis, Oregon, USA, [7]Institute of Biogeosciences, Japan Agency for Marine-Earth Science and Technology, Yokosuka, Japan, [8]Fukada Geological Institute, Tokyo, Japan

Abstract Brucite-carbonate chimneys were discovered from the deepest known (~5700 m depth) serpentinite-hosted ecosystem—the Shinkai Seep Field (SSF) in the southern Mariana forearc. Textural observations and geochemical analysis reveal three types (I–III) of chimneys formed by the precipitation and dissolution of constitutive minerals. Type I chimneys are bright white to light yellow, have a spiky crystalline and wrinkled surface with microbial mat and contain more brucite; these formed as a result of rapid precipitation under high fluid discharge conditions. Type II chimneys exhibit white to dull brown coloration, tuberous textures like vascular bundles, and are covered with grayish microbial mats and dense colonies of *Phyllochaetopterus*. This type of chimney is characterized by inner brucite-rich and outer carbonate rich zones and is thought to have precipitated from lower fluid discharge conditions than type I chimneys. Type III chimneys are ivory colored, have surface depressions and lack living microbial mats or animals. This type of chimney mainly consists of carbonate, and is in a dissolution stage. Stable carbon isotope compositions of carbonates in the two types (I and II) of active chimneys are extremely ^{13}C-enriched (up to $+24.1‰$), which may reflect biological ^{12}C consumption under extremely low dissolved inorganic carbon concentrations in alkaline fluids. Type III chimneys have ^{13}C compositions indicating re-equilibration with seawater. Our findings demonstrate for the first time that carbonate chimneys can form below the carbonate compensation depth and provide new insights about linked geologic, hydrologic, and biological processes of the global deep-sea serpentinite-hosted vent systems.

1. Introduction

Chemosynthetic ecosystems at deep-sea hydrothermal vents and seeps have been studied in the past decades to understand the diversity and limitations of life on Earth. Early studies focused on the on-axis hydrothermal fields in mid-ocean ridge (MOR) environments, which are characterized by high temperature (200–400°C), acidic (pH 2–6), and iron-rich and sulfide-rich fluids called "black smokers" [e.g., *Hannington et al*., 1995]. Microbial communities around black smoker systems have been considered as modern analogs for where life began on Earth, in part because microbes inhabiting the systems represent deeply branching lineages in the 16S rRNA gene phylogenetic tree [*Woese and Fox*, 1977] and in part because of the potential for ecosystems there to operate independently from photosynthesis [*Rasmussen*, 2000; *Ueno et al*., 2001, 2004, 2006; *Nakamura and Takai*, 2014]. However, since the discovery of the Lost City hydrothermal field (LCHF) off-axis site near the Mid-Atlantic Ridge [*Kelley et al*., 2001], low-temperature serpentinite-hosted hydrothermal systems have attracted great interest as another analog for the origin and early evolution of Hadean life [e.g., *Martin et al*., 2008] and as unique modern deep-sea chemosynthetic ecosystems [*Schrenk et al*., 2004; *Kelley et al*., 2005; *Brazelton et al*., 2006; *López-García et al*., 2007; *DeChaine et al*., 2006].

The LCHF vent fluids differ greatly from those of black smokers. These fluids are alkaline (pH 9–11), cooler (40–90°C), enriched with hydrogen (H_2) and methane (CH_4), and contain much lower concentrations of

metal and sulfide species [*Kelley et al*., 2001, 2005; *Seyfried et al*., 2015]. H_2 is produced via the serpentinization reaction [*Sleep et al*., 2004; *McCollom and Bach*, 2009], while CH_4 is subsequently produced by both microbial function (methanogenesis) and inorganic processes known as Fischer-Tropsch type reactions [e.g., *McCollom and Seewald*, 2001; *Charlou et al*., 2002; *Kelley et al*., 2005; *Proskurowski et al*., 2008; *Bradley and Summons*, 2010; *McCollom*, 2013]. H_2, CH_4, and other reduced organic compounds play a critical role in associated near-seafloor chemosynthetic microbial communities [*Kelley et al*., 2005; *Brazelton et al*., 2006; *Lang et al*., 2012], allowing chemosynthetic fauna to flourish [*DeChaine et al*., 2006; *Lopez-Garcia et al*., 2007].

Serpentinite-hosted or serpentinite-associated hydrothermal systems and serpentinite fluid seepages in the ocean have been reported from the Mid-Atlantic Ridge (LCHF, Rainbow, Logachev, Ashadze, and Nibelungen fields) (reviewed in *Schrenk et al*. [2013]), Central Indian Ridge (Kairei field) [e.g., *Nakamura et al*., 2009], Mariana forearc (Pacman, Conical, and South Chamorro Seamounts) [*Haggerty*, 1991; *Fryer*, 1996; *Yamanaka et al*., 2003; *Wheat et al*., 2010], and coastal springs in New Caledonia (Prony Bay hydrothermal field) [*Monnin et al*., 2014]. Nevertheless, there are only a few sites known to host relatively low-temperature ($<$100°C) and alkaline fluid discharges (LCHF and seep sites in the Mariana forearc serpentinite seamounts). The relatively few known examples of such systems are likely to reflect the difficulty of finding them, not their abundance in nature. In 2010, a new serpentinite-hosted chemosynthetic ecosystem was discovered on the landward slope of the southern Mariana Trench [*Ohara et al*., 2012]. The site was serendipitously found during the *Shinkai 6500* dive 6K#1234 in the YK10-12 cruise of the R/V *Yokosuka* [*Ohara et al*., 2012]. At this dive, vesicomyid clam communities were found on a slope exposing serpentinized peridotite at a depth of 5550–5810 m. In addition, a chimney fragment was recovered [*Ohara et al*., 2012]. The fragment contained brucite and carbonate [*Ohara et al*., 2012], similar to the chimneys found in some serpentinite-hosted systems at Pacman Seamount [*Fryer et al*., 1999], the LCHF [e.g., *Kelly et al*., 2001], and the Prony Bay hydrothermal fields [*Launay and Fontes*, 1985]. Although no active fluid discharge was observed during the dive, the site was named the "Shinkai Seep Field (SSF)," because the abundance of vesicomyid clam communities suggested that serpentinization-associated low-temperature alkaline seepage was likely to be supporting the chemosynthetic ecosystem [*Ohara et al*., 2012].

During subsequent expeditions (continuing yearly from 2013 to 2015), large chimney sites were discovered in the SSF at around 5700 m bsl. In this paper, we report the appearance, mineralogy, texture, stable carbon isotope composition of carbonates, and microbial and faunal colonization of the chimney structures of the SSF. Our study provides important insights into the geochemical and geobiological diversity of chimney mineralization and chemosynthetic ecosystem development in the global deep-sea serpentinite-hosted hydrothermal and seepage systems.

2. Geological Background

The SSF is located on the landward slope of the southernmost Mariana Trench, approximately 80 km northeast of the Challenger Deep (Figure 1a). The Mariana arc-trench system is a typical convergent plate margin where the Pacific Plate subducts beneath the Philippine Sea Plate. South of ~13°N, the southernmost Mariana arc-trench systems trends nearly E-W in contrast to the more N-S orientation of most of the Izu-Bonin-Mariana arc-trench system to the north. Forearc are important elements of an arc-trench system, and are generally characterized by a broad region between the trench axis and the associated volcanic arc. Along the Mariana forearc southwest of Guam, the West Santa Rosa Bank Fault (WSRBF) at approximately 144°15′E marks a major tectonic boundary [*Fryer*, 2003], dividing the Mariana forearc into northern and southern parts, which have very different appearances that reflect their different origins [*Ohara et al*., 2012]. In comparison to the broad forearc to the NE and further north, the southernmost Mariana forearc is deforming rapidly, including strong along-strike extension, allowing upwelling of weak, serpentinized forearc mantle [*Ribeiro et al*., 2013; *Stern et al*., 2013, 2014]. A number of serpentinite mud volcanoes (South Chamorro, Pacman, and Conical seamounts; Figure 1a) exist in the Mariana forearc to the north whereas serpentinized peridotite crops out on the inner trench slope along the southern Mariana forearc instead of forming serpentinite mud volcanoes; the difference probably reflects the fact that the northern forearc has been relatively stable for tens of millions of years, allowing fluid focusing and seamount growth whereas the southern forearc is tectonically much more active due to a combined effect of back arc opening of the Mariana Trough and the presence of a short and narrow Pacific Plate slab (a torn slab) below the WSRBF,

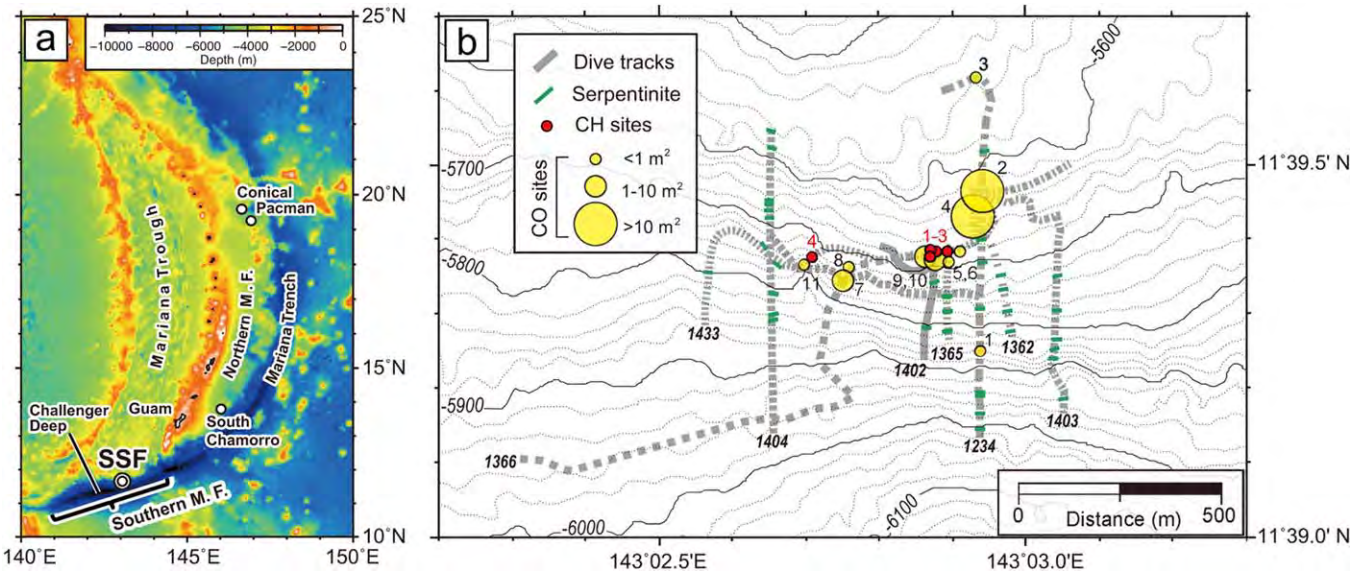

Figure 1. Location of the Shinkai Seep Field (SSF). (a) The SSF (double circle) located in the southern Mariana forearc (M.F.), northeast of the Challenger Deep. In the Northern M.F., active seeping sites occur atop large serpentinite seamounts (white circles). (b) Detailed locations of the 4 chimney sites (CH; red circles) and 11 vesicomyid clam sites (yellow circles) at the SSF with dive tracks (gray dashed lines) and occurrence of serpentinite mud veins (green lines; Figure 2a). The sizes of the yellow circles indicate the area distributing vesicomyid clam colonies (details in Table 1). Bathymetry was obtained with the Simrad EM122 multibeam sonar system installed on R/V *Yokosuka*.

and this slab is rolling back rapidly [*Gvirtzman and Stern*, 2004]. This results in serpentine-hosted vent systems that are much younger and more immature than those to the north.

3. Materials and Methods

3.1. Shinkai 6500 Dives at the SSF

The SSF was investigated by eight DSV *Shinkai 6500* dives (6K#1234, 6K#1362, #1365, #1366, #1402, #1403, #1404, and #1433) during four cruises of R/V *Yokosuka* (YK10-12, YK13-08, YK14-13, and YK15-11) from 2010 to 2015. The area of the vesicomyid clam colony sites was estimated from the captured video images using laser scales (20 cm apart). The sizes and volumes of the chimneys were roughly estimated with the scale of the laser markers on the capture images of each dive video (Figure 1b).

3.2. Sampling

Fragments of SSF chimney structures were collected using the manipulators of the *Shinkai 6500*. The chimney samples were collected from 11 structures. Faunas on the chimneys and the vesicomyid individuals were collected with a suction sampler into canisters, the outlet of which was covered with 1 mm mesh. In addition, the sediments were obtained from the colony sites by a scoop and push corers. Temperature was measured by a thermometer placed by the *Shinkai 6500* manipulator arm at fractures cross section of the collected chimneys, on the surface wall of standing chimneys, or just above vesicomyid colonies. The measurement error of the thermometer was $\pm$0.1°C.

The collected chimneys were sectioned onboard immediately after sample recovery. Chimney samples for textural observation and mineral identification were stored at 4°C. Biological samples were also subsampled for identification, and were fixed in either 99.5% ethanol or 4% formaldehyde-phosphate buffered saline solution, and then stored at 4°C onboard as soon as possible after recovery.

Because the SSF is located within the USA Mariana Trench Marine National Monument the investigations and samplings were done under the permission of US Fish and Wildlife Service (#12541-12001 for YK13-08, #12541-14001 for YK14-13, and #12541-15002 for YK15-11).

3.3. Chimney Descriptions

Mineral compositions of bulk chimney sample were determined by X-ray diffraction analysis (XRD; MiniFlexII, Rigaku Corp., Tokyo, Japan), with CuKα radiation (30 kV, 15 mA), and identified using automated peak

Table 1. Chimney and *Calyptogena* Colony Sites Found and Visited at the Shinkai Seep Field (SSF)[a]

Site	Dive No.	Cruise	Depth (m)	Location		Colony Scale (m^2)
Colony Sites						
CO Site 1*	6K1234	YK10-12	5861–5859	11°39.23′N	143°2.93′E	1
CO Site 2*	6K1234	YK10-12	5622	11°39.44′N	143°2.95′E	60
CO Site 3*	6K1234	YK10-12	5555	11°39.50′N	143°2.93′E	<1
CO Site 4	6K1362	YK13-08	5629	11°39.41′N	143°2.94′E	20
CO Site 5	6K1365	YK13-08	5692–5683	11°39.37′N	143°2.85′E	2
CO Site 6	6K1365	YK13-08	5682	11°39.37′N	143°2.85′E	<1
CO Site 7	6K1366	YK13-08	5740	11°39.33′N	143°2.74′E	1
CO Site 8	6K1366	YK13-08	5721	11°39.33′N	143°2.75′E	<1
CO Site 9	6K1366	YK13-08	5680	11°39.31′N	143°2.88′E	2
CO Site 10	6K1402	YK14-13	5683	11°39.36′N	143°2.87′E	1
CO Site 11	6K1404	YK14-13	5746–5741	11°39.36′N	143°2.67′E	1
			5555–5861		***Total***	***88***
						Chimney Vol. (m^3)
CH Site 1	6K1365	YK13-08	5683–5681	11°39.37′N	143°2.85′E	0.2
CH Site 2	6K1366	YK13-08	5687	11°39.31′N	143°2.88′E	3.3
CH Site 3	6K1402	YK14-13	5689–5683	11°39.36′N	143°2.88′E	8.0
CH Site 4	6K1404	YK14-13	5743	11°39.28′N	143°2.93′E	0.9
			5680–5743		***Total***	***12.4***

[a]Three colony Sites (*) have been reported in *Ohara et al*. [2012]. Localities were mapped in Figure 1b. Bold values show the depth ranges for colony and chimney sites and total values of colony sizes and chimney volumes.

search by PDXL software (Rigaku Corp.) at Japan Agency for Marine-Earth Science and Technology (JAMSTEC). The sampling points (whole or separation of outer and inner layer) for XRD analysis were determined on the basis of megascopic appearances. Proportion of the main mineral components, brucite ($Mg(OH)_2$), calcite ($CaCO_3$), and aragonite ($CaCO_3$) were determined with calibration curves of three binary mixtures of the standards (calcite-aragonite, calcite-brucite, and brucite-aragonite), following the methods of *Kontoyannis et al*. [1997]. The standard for calcite and aragonite was synthesized using the method of *Kontoyannis et al*. [1997]. A commercial product (99.9% $Mg(OH)_2$; American Element Inc., Los Angels, USA) was used as the brucite standard.

Saturation indexes for brucite, calcite, and aragonite in the ambient seawater at the SSF were calculated with a computer program, PHREEQC version 3 [*Parkhurst and Appelo*, 2013]. Seawater composition used for this calculation was actual measured values of the SSF ambient seawater obtained during dive 6K#1362. Major cation concentrations (Mg, Na, K, and Ca) were measured by an inductively coupled plasma-optical emission spectrometry (ICP-OES) with <5% of analytical error. Major anion concentrations (Cl and SO_4) were determined by an ion chromatograph (ICS-1600, DIONEX, CA) after 400 times dilution for Cl and 200 times dilution for SO_4. The alkalinity, pH, and the concentrations of SiO_2 were analyzed onboard. The pH and alkalinity were determined using a pH meter by potentiometric titration with 0.1 M HCl. SiO_2 concentrations were measured by calorimetric analysis described by *Gieskes et al*. [1991]. The analytical precisions were estimated to be within 0.5% for pH, 5% for alkalinity, and 7% for SiO_2. Pressure was set at 570 atm corresponding to 5700 m depth. Temperature was set at 1.6°C, which was measured in situ by the self-recording a thermometer during the dives.

The chimney samples were embedded into epoxy resin (E205, Konishi Inc., Osaka, Japan) to make thin sections for textural observation. The thin sections were observed with a polarized light microscope (Olympus BX-53, Tokyo, Japan) at JAMSTEC. The porosity of the chimney samples was measured by counting of the porous area in 10 microscopic views randomly selected in each thin section. For mineral identification of minerals in the thin sections, Raman spectra were obtained using a laser Raman microscope (RAMANtouch, Nanophoton Inc., Osaka, Japan) with nonpolarized 523 nm laser for excitation and a 300 g/mm diffraction grating at JAMSTEC.

Stable carbon isotopic compositions ($\delta^{13}C$) of the carbonate subsamples were determined using an isotope ratio mass spectrometer (GV Instruments IsoPrime) with an automated carbonate reaction system (Multiprep) at JAMSTEC. The $\delta^{13}C$ values are reported with respect to the Vienna Pee Dee Belemnite (VPDB) standard using standard delta notation in permill [*Craig*, 1957]. Analytical precision for the in-house carbonate standard was better than 0.06‰.

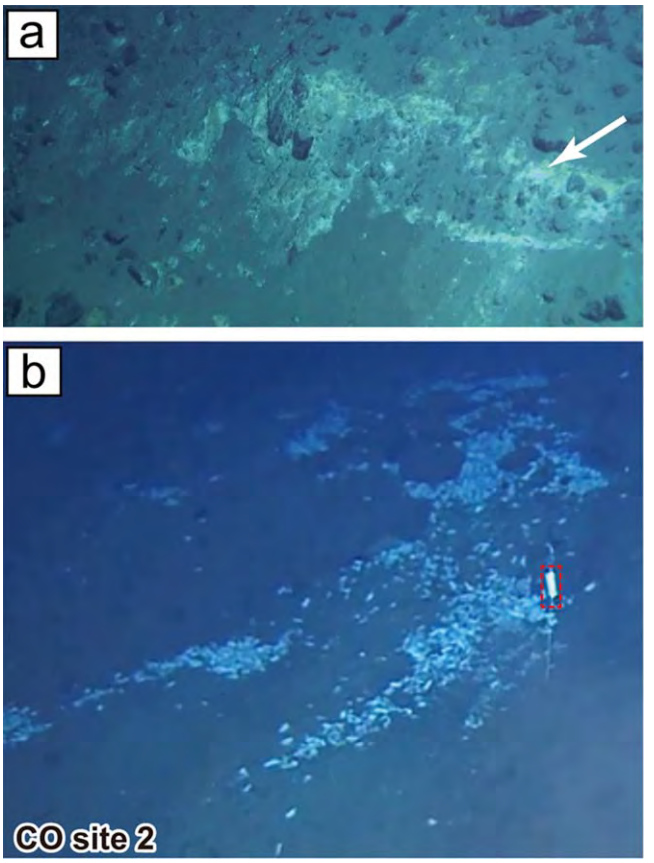

Figure 2. Overview of the colony (CO) sites at the SSF. (a) Near the colony sites, serpentinite-mud layers were frequently observed. (b) The largest colony sites (CO Site 2) are found in the eastern part of the SSF. The pale white areas are shells of *Calyptogena* (*Abyssogena*) *mariana*. The long axis of shells of *C. mariana* are ~10 cm. Red dashed square shows reflector of the marker set in this site during the dive 6K#1234. No chimney structures were observed in this site.

4. Results

4.1. Shinkai Dive Observations at the SSF

Figure 1b and Table 1 summarize the location of the vesicomyid clam colonies and chimney sites in the SSF. Each site was defined by an area where the colonies or the chimneys are concentrated. The sites were numbered in the order of their discoveries. At this time, only four chimney sites (CH Site 1–4) and 11 vesicomyid clam colony sites (CO Site 1–11) were found within an area of ~500 m square area centered at 11°39.36′N, 143°02.86′E (Figure 1b). They were located on a steep slope inclining south to southwest. The SSF seafloor consists of variably serpentinized peridotite covered with loose muddy to sandy sediments. Serpentine-mud layers were frequently observed in the seafloor covered with sediments (Figures 1b and 2a).

The colony sites (CO site 1–11) were observed at depths from 5861 to 5555 m (Figure 1b and Table 1). The colonies occurring on sandy and muddy seafloor were closely associated with serpentine mud layers (like Figure 2a). Two major colonies at 5622 m (CO Site 2; Figure 2b) and 5629 m (CO Site 4) appeared to have >20 m^2 areal extent. The other sites were sparsely distributed small colonies including 5–20 shells of vesicomyid clams, covering <2 m^2 areal extent. Some of the smaller colony sites were adjacent to the chimney sites, but no chimney structures were observed within the two major colony sites, CH Site 2 and 4 (Figure 1b and 2b). No fluid discharge was observed at the colony sites. Moreover, no temperature anomaly was detected around and just above the colony sites.

The four chimney sites had smaller areal extent than the colony sites (Figure 1b and Table 1). The sites were concentrated in two locations, at depths between 5680 and 5743 m (Figure 1b). Three chimney sites (CH Sites 1–3; Figures 3a–3d) were located close together, within a 40 m radius at the center of the SSF, while one site (CH Site 4; Figure 3e) occurred 300 m west away from the center chimney sites (Figure 1b). A video overview of the four chimney sites is shown in supporting information Movie S1. The total chimney volume is estimated to be 12.4 m^3 and 65% of this was found at the largest site, CH Site 3 (8.0 m^3 distributed in ~140 m^2; supporting information Movie S1). No fluid discharge was observed in situ or in recorded video images at any chimney site. Similar to the colony sites, no temperature anomalies were detected on the lower edges of chimneys or on the surface wall of standing chimneys.

4.2. Chimneys in the Shinkai Seep Field

4.2.1. Appearances

Chimneys of several cm to tens meters high grew upward from fractures in serpentinized peridotite outcrops or through thin overlying mud (Figures 3a–3d). Most chimneys have cylindrical or have sword-like shapes, because the chimneys align along cracks in the peridotite and at the interface between peridotite

and small overlying sediment ponds. Some chimneys growing from an over hanging peridotite cliff encrusted the cliff itself (supporting information).

We collected eleven chimney samples (Chim1–11), as summarized in Table 2. These chimney samples are grouped into three types based on color, texture, and biology:

Type I. Bright white to light yellow colored, spiky crystalline surface texture, with bushy white-gray, mushroom-shaped microbial mats (Figure 4a).
Type II. White to dull brown colored, with tuberous textures such as vascular bundles, and grayish microbial mat with a dense population of polychaetes in the genus *Phyllochaetopterus* (Figure 4b).
Type III. Ivory colored, smooth surface with hollows like karren (the denudation of karst), and lacking microbial mat or animals (Figure 4c).

The dominant chimney types vary among the chimney sites. Type I chimneys are abundant at CH Site 4, whereas type II chimneys are abundant at CH Sites 1 and 3. All chimneys at CH Site 2 are type III. Some chimney fragments were collapsed, adjacent to standing chimneys (Figure 2e and supporting information Movie S1). Most fallen chimneys and some standing chimneys were type III. Large chimney structures, over >5 m high, often appeared to have heterogeneous chimney types within a single structure, for example, type III distributing at the lower part, type II locally distributing at the middle part, and type I distributing at the top in a single chimney (supporting information Movie S1). We collected 11 chimney samples (Chim1–11) as summarized in Table 2. Representative chimneys of each type are shown in supporting information Movie S1.

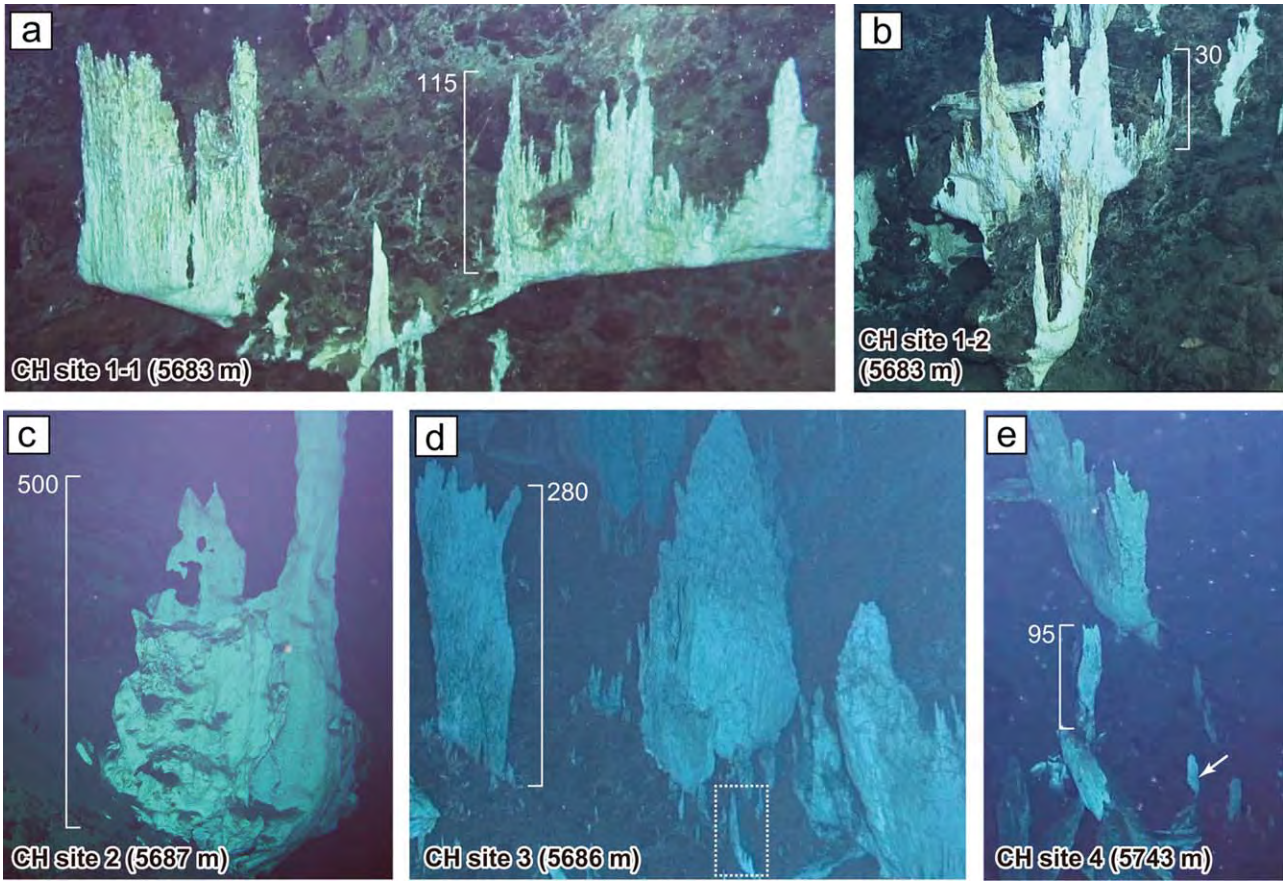

Figure 3. Overview of the chimney sites at the SSF. White bars and numbers in each plot indicate the height of the chimneys in cm. (a and b) Chimneys at CH Site 1 are growing from a joint in serpentinized peridotite cliff. (c) A large chimney structure observed at CH Site 2. Overall length of the structure is over 5 m. (d) A part of the largest chimney site (~140 m^2) at CH Site 3. Dashed square shows a chimney sampling point that is corresponding to Figure 10b. (e) CH Site 4 situated at the west side of the SSF area. The chimney indicated by white arrow corresponds to the chimney numbered "5" in top plot of Figure 10a. Overview of each chimney sites is shown in supporting information Movie S1.

Table 2. Chimney samples recovered from the Shinkai Seep Field

	Sample ID (SUP#_Dive#-ID#)	CH Site	Depth (m)	Surface	Color	Typical Biology	Type
Chim1	6K1234-R02		6079	Smooth	Iv		III
Chim2	12541-12001_6K1365-R01, 02, 03	1	5683	Smooth and tuberous	WH, DB	Microbial mat and polychaetes	II
Chim3	12541-12001_6K1366-R03, 04	2	5687	Smooth	Iv	None	III
Chim4	12541-14001_6K1402-R01	3	5683	Tuberous	WH, DB	Microbial mat and polychaetes	II
Chim5	12541-14001_6K1404-R04	4	5743	Crepey	WH, DB	Mushroom microbial mat	I
Chim6	12541-14001_6K1404-R05	4	5743	Spiky	BWH	White cottony microbial mat	I
Chim7	12541-15002_6K1433-R01	4	5743	Spiky	BWH	Microbial mat	I
Chim8	12541-15002_6K1433-R02, 03	4	5743	Spiky	BWH	White bushy microbial mat	I
Chim9	12541-15002_6K1433-R04	4	5743	Spiky	BWH	Microbial mat	I
Chim10	12541-15002_6K1433-R05-t	3	5743	Tuberous	WH, DB	Microbial mat and polychaetes	II
Chim11	12541-15002_6K1433-R05-n	3	5743	Spiky	BWH	Microbial mat	I

4.2.2. Mineralogy

XRD analysis shows that the SSF chimneys consist chiefly of brucite, calcite, and aragonite (Figure 5 and Table 3). The proportions of the three mineral components differ among the chimney types and sampling sites. Most type I chimney samples contain >80 wt % brucite. A sample from the root of a type I chimney contained ~60 wt % calcite and 40 wt % brucite. Aragonite is a minor component of type I chimneys (Figure 5). Type II chimneys have more calcite than do type I chimneys (Figure 5). Heterogeneous mineralogy is characteristic of type II chimneys; the outer part mainly consists of calcite and aragonite with minor brucite (<20 wt %). Brucite zonation characterizes type II chimneys, with minor brucite on the outside, but abundant brucite on the inside. Aragonite content in the outer part of type III chimneys is up to 93 wt % (Table 3).

PHREEQC calculations show that the ambient seawater at the SSF site is undersaturated in brucite, aragonite, and calcite. The results and parameters used for the calculation are summarized in Table 4. This modeling indicates that the chimneys cannot exist without continuous mineral growth sustained from serpentinite fluid discharge. These results also indicate that brucite in particular will redissolve once the discharge stops.

In addition to these main mineral contents, possible ikaite were observed in type II chimneys. Rhombohedral crystals a few mm long axis locally occurring within the inner porosity of the type II chimney (Figure 6a). This crystal dissolved in 10% HCl (Figure 6b). In addition, the crystal decomposed with leaking a cloudy white fluid within 12 h at room temperature. These features indicate that the crystals are likely the unstable hydrated carbonate phase ikaite ($CaCO_3$-$6H_2O$).

4.2.3. Textures

The three chimney types (I–III) exhibit different micro textural components.

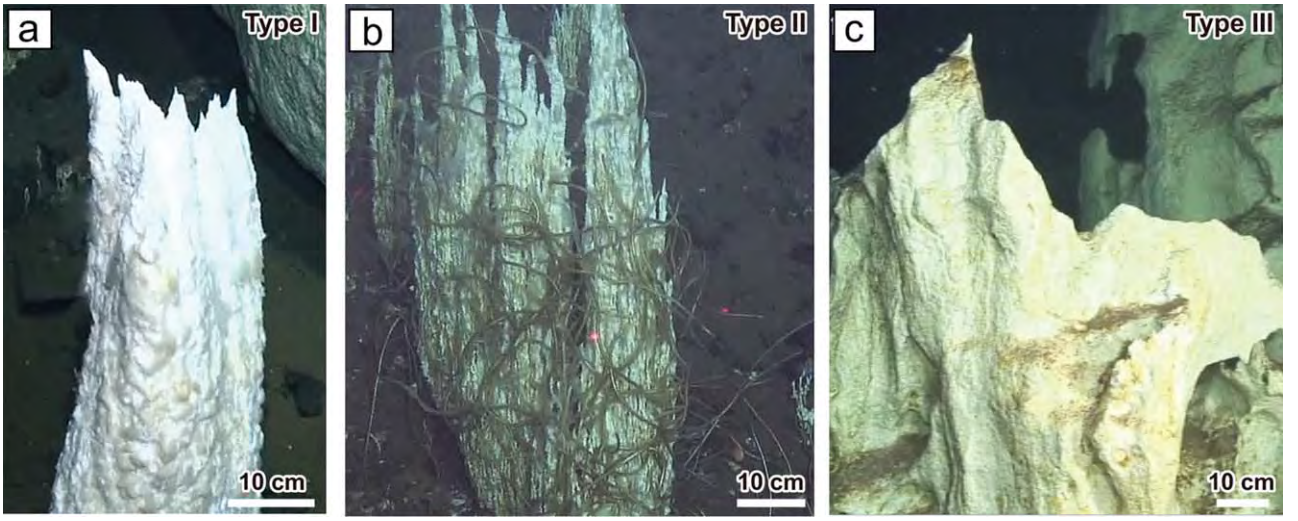

Figure 4. Three types of chimneys at the SSF. (a) A type I chimney at CH Site 4 with bright white spiky surface and cottony microbial mat. (b) A type II chimney at CH Site 3 with dull white surface densely covered by aggregated polychaetes. (c) A type III chimney at CH site 2 showing a smooth surface with depression and lacking microbial mat or animals.

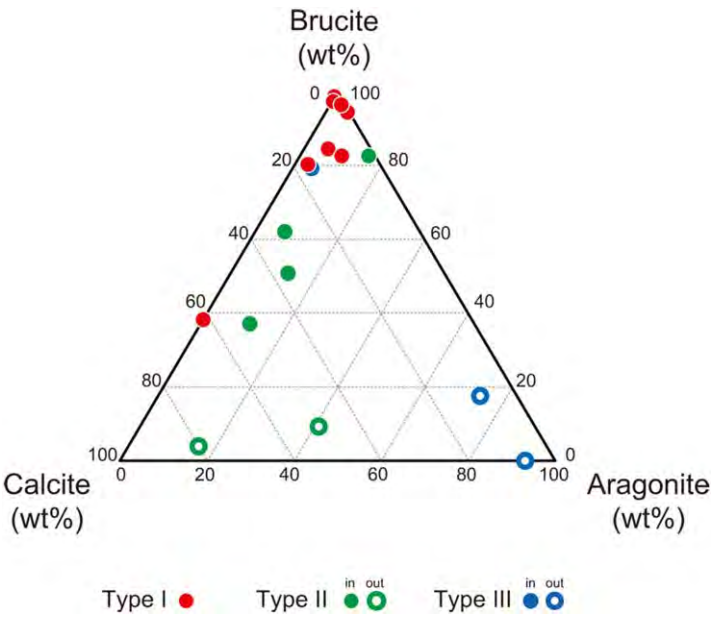

Figure 5. Mineralogy of the three types (red: type I, green: type II, and blue: type III) of SSF chimneys shown on a brucite-calcite-aragonite triangular diagram. "in" = inside of chimney, "out" = outside of chimney.

Type I chimneys showed spiky crystalline surface consisting of vertically elongated acicular structures (Figure 7a). The vertical section exhibits flame-like mineral aggregations with high porosity (42–59%) (Figure 7b). These aggregations consist of microcrystalline brucite and euhedral calcite crystals. Microcrystalline brucite comprised sinuous tubular structures ranging from ~80 to ~500 μm (Figures 7c and 7d). Walls of these structures consist of stacks of isopachous layers ~10 μm thick (Figure 7d), while parts of the brucite walls show convex to conoform microbialite structures (Figure 7e). Microcrystalline brucite also aggregates in forms of reticular texture (Figures 7d and 7f), the framework of which is composed of filamentous microbial cells 3.5–4.5 μm in diameter (Figure 7g). Such microbial cells were also observed in the layered walls (Figure 7d). Polygonal calcite crystals occur on the tubular structures or fill voids in the tubules. Calcite occurs as polygonal and euhedral crystals from several tens of μm to 400 μm a side length (Figures 7c and 7d). This indicates that the polygonal calcite crystals precipitated after the brucite. The size of polygonal calcite crystals increases with increasing abundance of calcite.

Type II chimneys show porous (41–56% porosity) textures like vascular bundles, which consist of sinuous tubular structures (Figures 8a–8c) with two types differing in diameter. The smaller tubules range from 0.5 to 5 mm, while the larger tubules range from 5 to 8 mm (Figures 8b and 8c). The smaller tubular structures in type II chimneys are considered to be relict fluid flow conduits and are one order magnitude larger than those in type I chimneys (Figures 7c and 7d). The inner wall of the smaller tubular structure consists of

Table 3. Mineral Composition of the Chimney Samples Collected From the SSF[a]

			Mineral Composition		
Sample	Type	Subsampling Site	Brucite (wt %)	Calcite (wt %)	Aragonite (wt %)
Chim1	III	Outer1	0	7	93
Chim1	III	Outer2	18	9	73
Chim1	III	Inner	79	17	4
Chim2	II	Inner	62	31	7
Chim2	II	Outer1	9	50	41
Chim2	II	Outer2	4	80	16
Chim3	III	N			
Chim4	II	Middle	37	52	11
Chim4	II	Root	82	2	16
Chim5	I	Root	38	62	0
Chim6	I	Whole	98	2	0
Chim7	I	Whole	80	17	3
Chim8	I	Whole1	99	1	0
Chim8	I	Whole2	94	1	5
Chim9	I	Whole1	83	8	9
Chim9	I	Whole2	85	10	5
Chim10	II	Whole	51	36	13
Chim11	I	Whole	96	1	3

[a]The details of the samples are described in Table 2.
N; XRD analysis did not perform due to small amount of samples.

Table 4. Ambient Seawater Compositions and Saturation Indexes for Brucite, Calcite, and Aragonite at the SSF, Which Were Calculated Using PHREEQC

	Value	Unit
Parameters (Ambient Seawater)		
Ca^{2+}	425	mg/L
Mg^{2+}	1263	mg/L
Na^{+}	10984	mg/L
K^{+}	404	mg/L
Cl^{-}	19488	mg/L
SO_4^{2-}	2712	mg/L
SiO_2	3.7	mg/L
Alkalinity	128	mM
pH	7.8	
Pressure	570	Atm
Results		
$SI_{brucite}$	−3.88	
$SI_{calcite}$	−0.27	
$SI_{aragonite}$	−0.40	

microcrystalline brucite, while the outer wall is calcite (Figures 8d and 8e). The larger tubular structures are tubes of *Phyllochaetopterus*, polychaetes embedded into the chimneys (Figure 8a). Interstices between these tubules are filled with various morphologies of brucite and anhedral calcite (Figures 8d and 8e). Some of the microcrystalline brucite is built of convex, conoform microbialite structures (Figure 8f) in both type I and type II chimneys (Figure 7e). No polygonal euhedral calcite crystals occur in type II chimneys (Figures 8d and 8e). Furthermore, mineralized microbial cells are exceedingly scarce in type II chimneys. The outer part of type II chimneys consists of random aggregations of large (>500 μm long) rhombic calcite and needle aragonite (Figure 8g). This surface layer unconformity cut the inner tubular structure (Figure 8g). Thickness of the outer carbonates layer ranges from a few mm to cm (Figure 8g).

Type III chimney mainly consists of the same texture as that found in the outer carbonate layer in type II chimneys (Figure 8g). Needle-like aragonite crystals dominate in the outer part of type III chimneys (Figure 9). There thus seems to be a continuum from Type I brucite chimneys evolving with decreased venting to Type II (inner brucite, outer carbonate) to Type III (calcite) chimneys reflecting progressive replacement of brucite by carbonate.

4.2.4. Carbon Isotopic Ratio

The results of isotope analysis of SSF chimney carbonates are summarized in Figure 10 and Table 5. Some references are also shown; carbonates at marine serpentinite-hosted systems such as Conical Seamount [*Haggerty*, 1991; *Kato et al*., 1998], South Chamorro Seamount [*Haggerty*, 1991], Ghost City carbonate [*Lartaud et al*., 2011], the LCHF [*Kelley et al*., 2005], and Iberian Margin [*Schwarzenbach et al*., 2013].

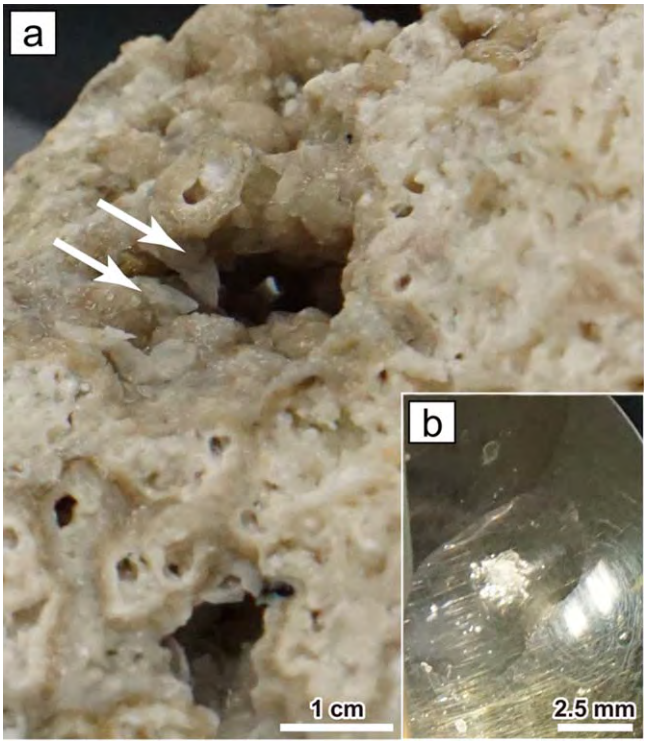

Figure 6. A minor mineral, potential ikaite, observed on-board the research vessel straight after sampling. (a) Potential ikaite minerals ($CaCO_3{\cdot}6H_2O$ rhombohedra indicated by white arrows) in the porous area of a type II chimney. (b) Close-up of the rhombohedral crystals, which dissolved in 10% HCl.

$\delta^{13}C$ of the SSF chimney carbonates show large variability and extremely high values compared to other sites (Figure 10). They range from −8.8 to +23.6‰ in type I chimneys, −0.3 to +24.1‰ in type II chimneys, and +1.0 to +1.4‰ in type III chimneys (Figure 10). $\delta^{13}C$ of type III chimneys and the outer carbonate layer of type II chimney are similar to the value of dissolved inorganic carbon (DIC) in seawater, ~0‰. Higher $\delta^{13}C$ values occur in the inner parts of type I and II chimneys with lower porosity (~40% porosity). The lowest $\delta^{13}C$ value (−8.8‰) is from inside a type I chimney.

The SSF records a wider range in $\delta^{13}C$ values (−8.8 to +24.1‰) than the other carbonates at marine serpentinite-hosted systems (Figure 10). The highest value, +24.1‰, is ~10‰ higher than the highest values from the LCHF. Such ^{13}C-enriched values were reported from authigenic carbonates in sediment cores recovered from continental margins [e.g., *Naehr et al*., 2007], but these are not a serpentinite-hosted system.

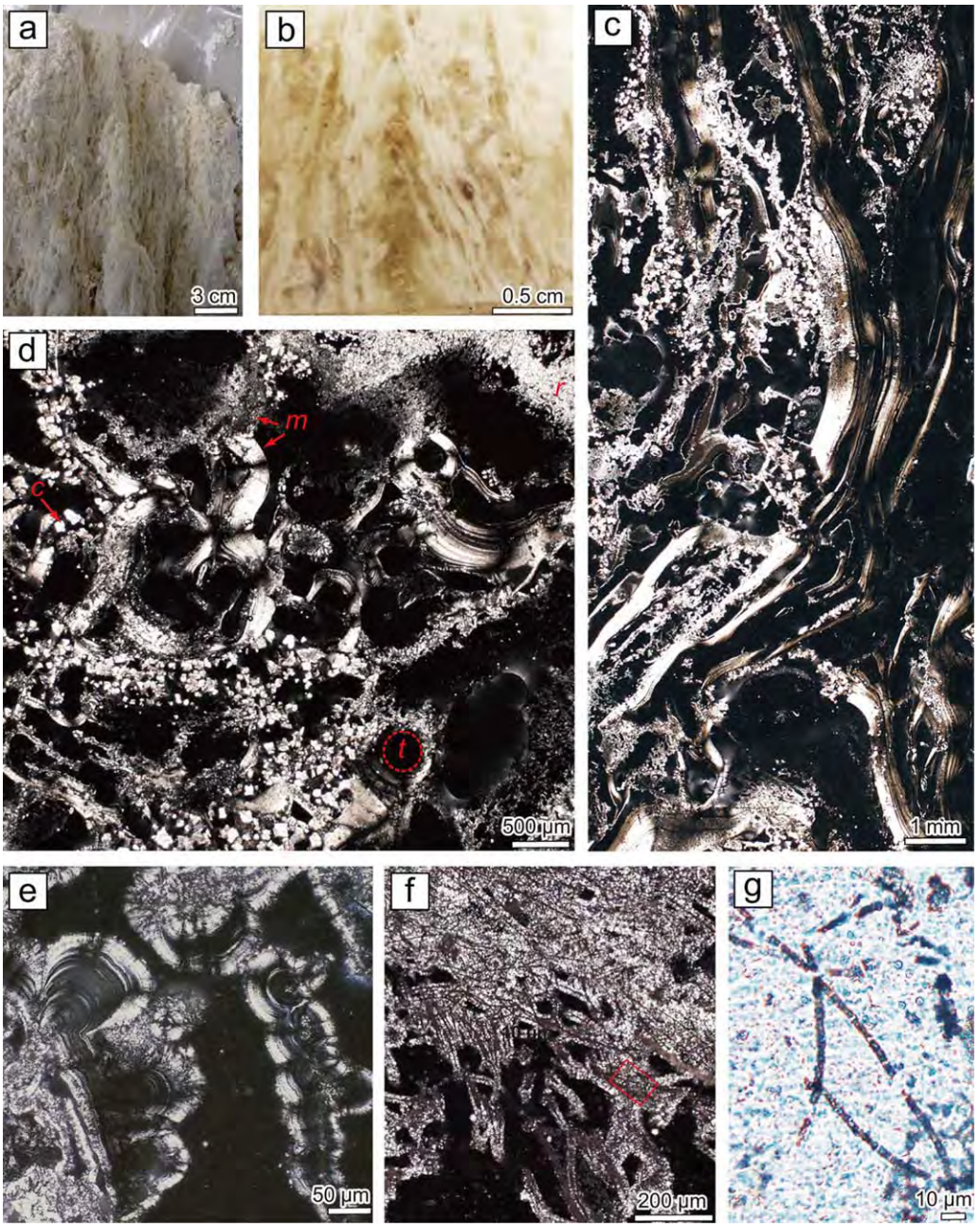

Figure 7. Texture of the type I chimney at the SSF. (a) Spiky surface consisting of upward-elongated aggregated spindles of brucite. (b) Vertical section of the resin-embedded samples. (c) Cross-polarized vertical thin section. (d) Cross-polarized horizontal thin section image. Precipitates consist of microcrystalline brucite (*m*) and euhedral calcite (*c*). Microcrystalline brucite forming tubular structure (*t*) and reticular texture (*r*). (e) Cross-polarized horizontal thin section image showing the conoform microbialite structures. (f) Close up of cross-polarized view in the reticular texture. Red dashed square indicates the area of Figure 7g. (g) Unpolarized photomicrograph of core of the reticular structure. Filaments of microbial cells are mineralized.

4.2.5. One Year Growth of SSF Chimneys

During dive 6K#1433, we revisited the same sampling points at CH Sites 3 and 4 as in the previous dives of 6K#1402 and 6K#1404, respectively, and observed the changes over 1 year in the chimney structures. Although the original chimney types were different, all of the newly grown chimneys showed uniform appearance consistent with type I category (Figures 11a and 11b). Newly grown chimneys range from several cm to ~30 cm high (Figures 11a and 11b). The newly grown chimneys are also shown in supporting information Movie S1. Total volumes of new chimneys were estimated from the dive video images as ~250 cm^3

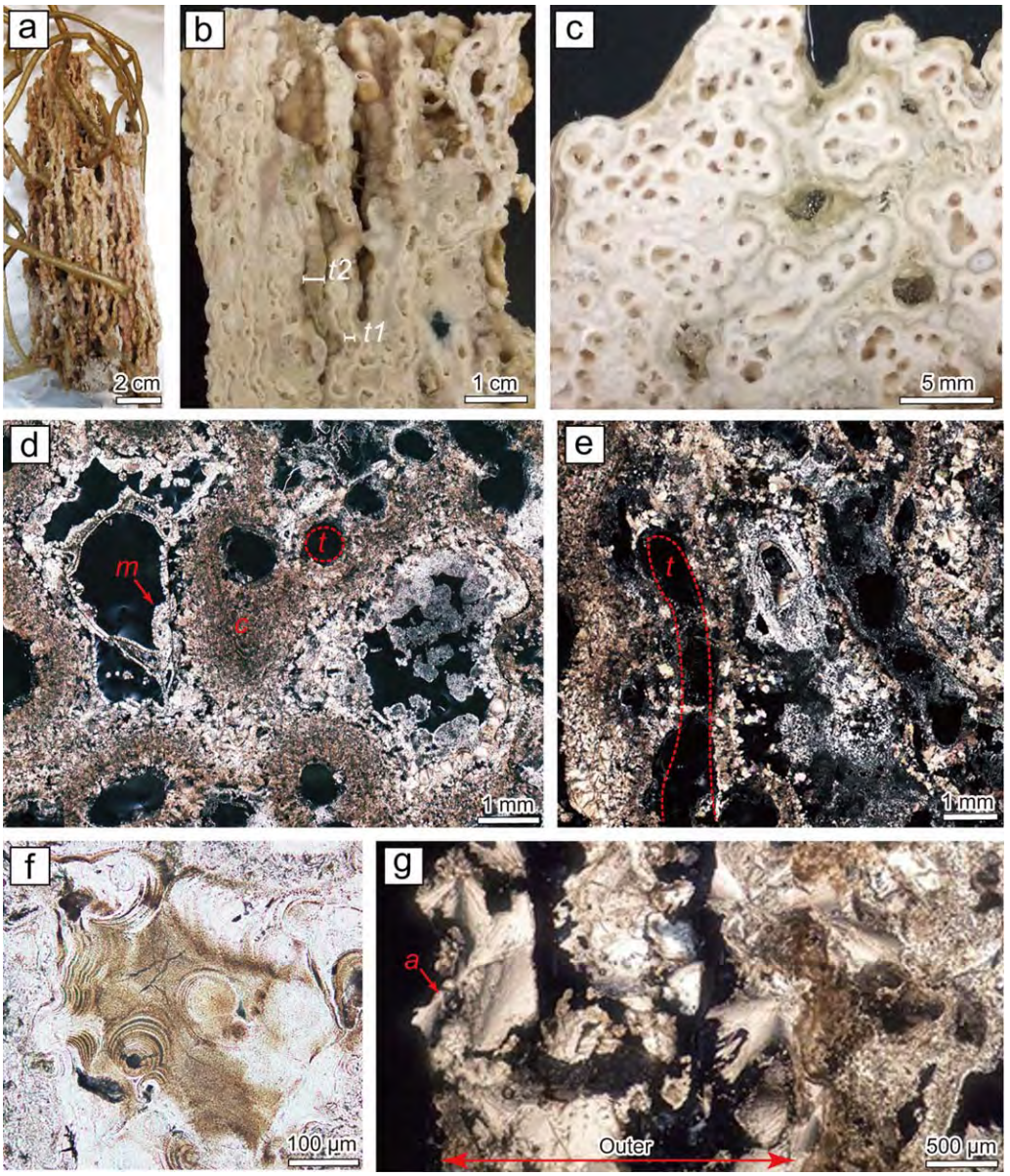

Figure 8. Textures of SSF type II chimneys. (a) Type II chimney structure, consisting of bundles of tube structures. Some polychaete tubes are embedded in the chimney. (b) Vertical section of polished cut surface. The smaller tube structures (*t*1) may be fluid conduits. The larger tube structures (*t*2) are embedded polychaete tubes. (c) Horizontal section of the resin-embedded samples. (d) Cross-polarized photomicrograph of horizontal section. The Bright inside part of the tube structure (*t*) having consists of microcrystalline brucite (*m*), while the outside consists of anhedral micrilic calcite (*c*). (e) Cross-polarized photomicrograph of vertical section. The smaller tube structure (*t* and red dashed line) elongates upward in an undulating manner. (f) Unpolarized photomicrograph section through conoform microbialite structures. (g) Cross-polarized photomicrograph of a vertical section through a type II chimney surface. The outer ~1.5 mm of the chimney (white arrow) consists of large needle-like aragonite crystals (*a*) that are randomly elongated.

at CH Site 3 and ~1200 cm^3 at CH Site 4. Approximate areas of fractures cross section of chimneys after sampling with the newly grown chimneys in CH Sites 3 and 4 were 45 cm^2 and 90 cm^2, respectively. From the volumes, porosities, and mineral compositions, brucite and carbonate precipitation rates were estimated. The values used and the results are summarized in Table 6. Brucite precipitation rate at CH Site 4 (9.9×10^{-10} mol cm^{-2} s^{-1}) was about 2 times larger than that at CH Site 3 (4.7×10^{-10} mol cm^{-2} s^{-1}). Carbonate precipitation rates at CH Site 4 (6.3×10^{-11} mol cm^{-2} s^{-1}) was 2.5 times that at CH Site 3 (2.6×10^{-11} mol cm^{-2} s^{-1}).

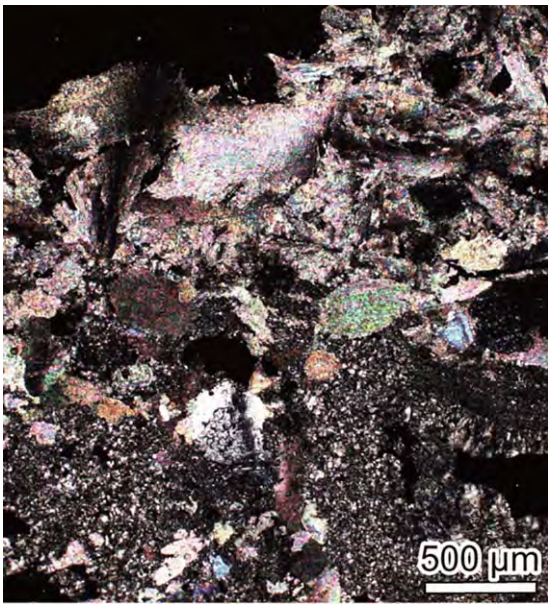

Figure 9. Textures of SSF type III chimneys. Cross-polarized photomicrograph of the vertical section showing mosaic aggregation of the large needle-like crystals similar to the outer carbonate layer of the type II chimney (Figure 8g).

4.2.6. Faunas in the SSF

In situ observations and onboard and onshore characterizations show the occurrence of chemosynthetic faunal communities in the SSF. Previously reported animals such as *Calyptogena* (*Abyssogena*) *mariana* clams [*Okutani et al.*, 2013], actiniarians, zoanthids, *Beroe* comb jelly, buccinid snail *Bayerius* cf. *arnoldi*, and galatheid crab (*Munidopsis* sp.) [*Ohara et al.*, 2012] were also observed at the two major colonies (CO Sites 2 and 4) during subsequent expeditions (Figure 12a). *Calyptogena mariana*, nautiliniellads, siboglinids, and ophiuroids were only collected from colony sites. Isopods, actiniarians, amphipods, polychaetes (including maldanids), *Bayerius* cf. *arnoldi*, and *Munidopsis* sp. squat lobsters were collected from both the central regions of colonies and the surface of chimneys using suction sampler. In addition to these common faunas, nebaliaceans, *Phyllochaetopterus* sp., polynoids, actinostolids, and a number of gastropods (*Provanna* sp., Xylodisculidae gen et sp., Trochoidea indet.) were collected only from chimney surfaces. Faunal communities on type II chimneys at CH Sites 1 and 3 were characterized by dense population of *Phyllochaetopterus* sp. on the type II chimneys (Figure 12b). *Phyllochaetopterus* sp. was densely entangled on the chimneys at CH Site 3, but only sparsely on type I chimney at CH Site 1 (Figures 4a and 4b). A gastropod, *Provanna* sp., showed localized distribution in type II chimney at CH Site 3. It was found only in the inner surface, but not on the outer surface of the chimney (Figure 12c). *Provanna* is a genus endemic to chemosynthetic ecosystems, the present species is described as a new species and appears to be a deposit feeder (Chen et al., unpublished data). Fauna on type I chimney was simpler than that on type II chimneys. Galatheid crabs and polynoids were the only animals large enough to be observed in situ but a few species of amphipods as well as polychaetes were obtained from washings. As described in the previous section on the chimney appearances, no animals were observed on type III chimney at CH Site 2 (Figure 4c).

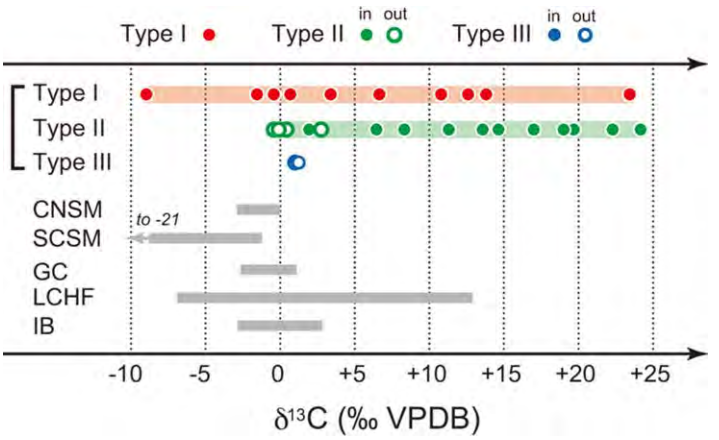

Figure 10. $\delta^{13}C$ values of SSF chimney samples compared to some other carbonate precipitates. Type I (red circles) and type II chimneys (green circles) show wider ranges of $\delta^{13}C$ than type III chimneys (blue open circles). The references are as follows: CNSM; Conical seamount, SCSM; South Chamorro seamount, GC; Ghost City carbonate, LCHF; Lost City hydrothermal field, and an Ocean Drilling Program site of Legs 149 and 173 at Iberian Margin. Values and each references summarized in Table 5.

5. Discussion

The brucite-carbonate chimneys have been obtained from ~5700 m depth on a forearc slope exposing serpentinites in the southern Mariana Trench. Here is the new deepest vent field deeper than the Beeve vent field on the mid-Cayman Rise, at around 4960 m, which is the deepest known vent field (*Kinsey and German*, 2013; *Webber et al.*, 2015). The SSF is the only serpentinization-associated brucite-carbonate chimney site known to occur below the local carbonate compensation depth (CCD, ~4500 m bsl) [*Seibold and*

Table 5. Carbon Isotope Values of the Three Types of SSF Chimneys With Some References

		δ^{13}C (‰ VPDB)		
	n	min.	max	Ref.
SSF Type I	13	−8.8	+23.6	This study
SSF Type II (inner)	12	+2	+24.1	This study
SSF Type II (outer)	8	−0.3	+2.9	This study
SSF Type III	6	+1	+1.4	This study
Conical Seamount		−2.9	0.1	1, 2
South Chamorro Seamount		−21.2	−1.2	1
Ghost City		−2.59	+1.09	3
Lost City		−7	+13	4
Iberian Margin		−2.9	+2.8	5

Ref. (1) *Haggerty* [1991], (2) *Kato et al.* [1998], (3) *Lartaud et al.* [2011], (4) *Kelley et al.* [2005], (5) *Schwarzenbach et al.* [2013].

Berger, 1996]. As shown by the PHREEQC calculation, the ambient seawater at the depth of the SSF is undersaturated in both brucite and carbonates (calcite and aragonite). Brucite-carbonate chimneys cannot exist without fluid input leading to brucite and carbonates precipitation.

Although the actual mineral dissolution rates have not been measured in situ at the SSF, we can roughly calculate the residence time of the chimney structure with some available data and assumptions. Assuming that the bulk chimney structure in the SSF is a cuboid consisting of cubic crystals with a side length of 100 μm, amount of brucite and carbonate (mol) and the bumpy surficial area (cm^2) could be roughly estimated by using measured values of the average porosity (50%), mineral composition (60% brucite and 40% carbonates). $CaCO_3$ dissolution rates in deep-sea settings (∼5000 m depth) have been measured to be 0.7–5.4 × 10^{-13} mol cm^{-2} s^{-1} [*Peterson*, 1966; *Milliman*, 1977; *Berelson et al.*, 1990]. Brucite dissolution rates have only been constrained by laboratory experiments that are not strictly applicable to the deep-sea setting, for example, ∼10^{-12} mol cm^{-2} s^{-1} at 1 atm, 25°C, pH = 8, and 0.01 mol/L NaCl [*Pokrovsky and Schott*, 2004], and ∼5.0 × 10^{-13} mol cm^{-2} s^{-1} at 1 atm, 22–25°C, pH = 8 [*Kudoh et al.*, 2006]. Details of the calculation are summarized in Table 7. The calculation indicates that the observed total of 12.4 m^3 of SSF chimneys would dissolve within 4–30 years (assuming no fluid flux from vents). This is a tentative and rough assumption, but it does support our conclusion that there is active—if cryptic—fluid flow from vents.

Mineralogy of the SSF chimneys provides important clues for the yet unknown physical and chemical properties of discharging fluids. We have not detected significant temperature anomalies in the SSF chimney sites, but the fact that especially Type I chimneys continue to grow indicates significant flow of a distinct fluid from the seafloor. Brucite is the primary precipitate and is only stable in alkaline solutions [*Pokrowsky and Schott*, 2004]. Occurrence of possible ikaite is another important indicator of alkaline solutions, because it is usually found in cold (<4°C) and alkaline environments [*Buchardt et al.*, 1997; *Rickaby et al.*, 2006, *Hu et al.*, 2014]. Ikaite is also found in the active portion of the chimney structures at the LCHF [*Ludwig et al.*, 2006], which is precipitated from highly alkaline (up to pH = ∼12) hydrothermal water. We conclude that the SSF chimneys precipitated from low-temperature alkaline fluids accompanied by variable mixing with seawater. No fluid discharge was observed during the previous expeditions, which was however probably due to the fluid venting being too weakly, diffusively, episodically, or all of the above.

The in situ observation of growth of chimneys at the same sampling points for 1 year (Figures 11a and 11b) is compelling evidence for on-going fluid seeping. Moreover, the comparison of mineralogies, textures, and structures of newly grown (type I), mature (type II), and dead (type III) chimneys reflects temporal variations of fluid discharges and re-equilibration with ambient seawater. All newly grown chimneys are type I chimneys, irrespective of the types of their host chimney structures (whether type I or II; Figures 11a and 11b). New chimneys are dominantly (>80%) brucite (Table 3 and Figure 5). A geochemical simulation for chimney formation at the LCHF predicts that more brucite forms when there is a greater proportion of alkaline fluid in the mixing zone between the hydrothermal fluid and ambient seawater [*Palandri and Reed*, 2004]. These results suggest that formation of different morphological and mineralogical types of chimneys reflects the mineral precipitation rate, which is tightly coupled with the input (discharge rate) of alkaline serpentinite-derived fluid. For example, brucite-dominated type I SSF chimneys form rapidly with high fluid discharge rates while the carbonate-dominated type II chimneys form more slowly under lower fluid discharge conditions. This is consistent with the estimated precipitation rates of different chimney sites (Table 6); about 2 times lower precipitation rate at CH Site 3 with dominant type II chimneys than at CH Site 4 with dominant type I chimneys. In addition, the abundance of mineralized microbial cells in type I but not in type II chimneys (Figure 7g) indicates better preservation of primary textures and also supports the hypothesis that

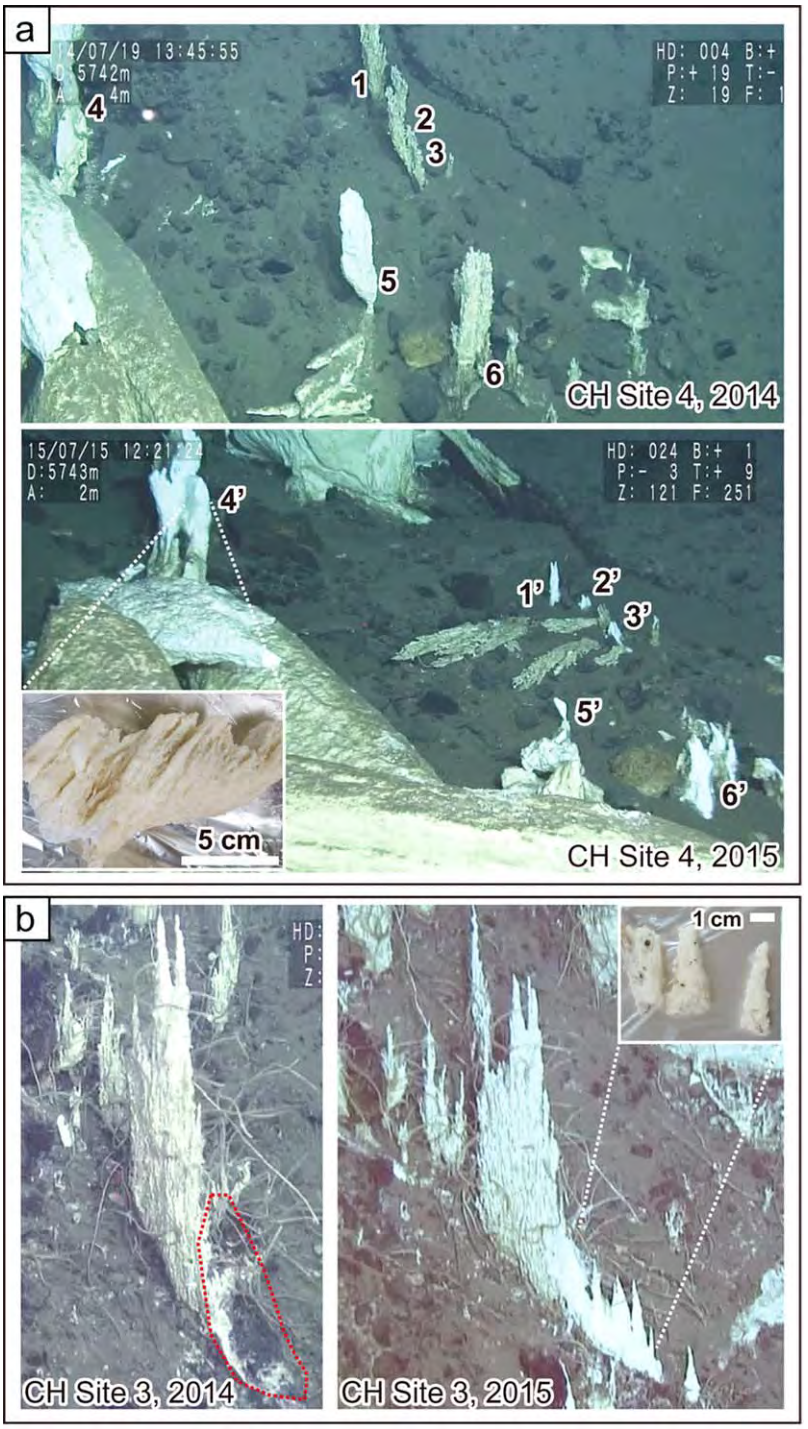

Figure 11. Newly grown chimneys observed during *Shinkai 6500* dive 6K#1433 on YK15-11 cruise. (a) The top plot shows type I chimneys at CH Site 4 in 2014 before sampling during dive 6K#1404. The bottom plot shows six new chimneys (1′–6′) observed in 2015 during dive 6K#1433. A sample obtained from the structure labeled 4′ was type I chimney and the newly formed chimneys was also type I. This corresponds to Chim8 in Table 2. (b) The left plot shows the appearance of a type II chimney at CH Site 3 after sampling during dive 6K#1402 in 2014. Basement rock was exposed fracture cross-section of chimney after sampling (red dashed outline). The right plot shows newly grown bright white chimneys at that the fracture cross section, observed and collected during dive 6K#1433 in 2015. These bright white structures were type I chimneys (small window in the right plot).

type I chimneys more rapidly precipitate. In order for microbial cells to be preserved, mineralization must have occurred at the same time as the cells grew, or immediately after their death and before the cell degraded.

Type III chimneys are secondary replacements of primary mineralization after alkaline fluid input ceased. Large crystals of calcite and aragonite in type III chimneys and the outer layer of type II chimneys (Figure 8g) are considered to be secondary replacements of primary brucite as the first stage in dissolving SSF chimneys. Brucite is strongly undersaturated in seawater and is replaced by carbonate soon after it is isolated from alkaline vent fluids, which can result when the vent stops flowing or by continued growth of brucite in a chimney above an active vent. Brucite reacts rapidly with seawater because the saturation index for brucite ($SI_{brucite} = -3.88$) is smaller than those of aragonite ($SI_{aragonite} = -0.40$) and calcite ($SI_{calcite} = -0.27$), as shown by the PHREEQC calculation (Table 4). Brucite dissolution elevates circumambient fluid pH, which triggers subsequent carbonate precipitation as follows:

$$Mg(OH)_2 \rightarrow Mg^{2+} + 2\ OH^- \quad \text{(Brucite dissolution)}$$

$$Ca^{2+} + HCO_3^- + OH^- \rightarrow CaCO_3 + H_2O \quad (CaCO_3 \text{ precipitation})$$

Various physicochemical factors control formation of the $CaCO_3$ polymorph, however aragonite tends to precipitate under high molar ratio of Mg/Ca (>1) [e.g., *Murray*, 1954; *Folk*, 1974, 1994]. Higher proportion of replacement aragonite (20–93 wt %; Figure 5) likely resulted from precipitation under high Mg/Ca ratio due to brucite dissolution.

The carbon isotope values of carbonate in the SSF chimneys are also consistent with secondary carbonate precipitation during the dissolution stage. The $\delta^{13}C$ values of carbonates in type III chimneys and outer layer of type II chimneys are close to that expected for seawater, $\sim 0‰$ (Table 5 and Figure 9). In contrast, a much wider range of $\delta^{13}C$ values (-8.8 to $+24.1‰$) characterize type I and inside layer of type II chimney samples. This indicates the involvement of a vent fluid that has ^{13}C-depleted and/or ^{13}C-enriched DIC for carbonate precipitation.

The ^{13}C-enriched values ($\delta^{13}C$ up to $+24.1‰$) of carbonate in the SSF chimneys are especially interesting. Similar highest values of carbonate $\delta^{13}C$ (up to $+26‰$) have been reported from authigenic carbonates in sediments at continental margins [*Sample and Kopf*, 1995; *Greinert et al*., 2001; *Orphan et al*., 2004; *Naehr et al*., 2007]. In these systems, the ^{13}C-enriched DIC originated from the zone of methanogenesis, where CO_2 reduction in a closed system pushed the carbon isotopic composition of pore water DIC up to $\sim +40‰$ [e.g., *Chatterjee et al*., 2011]. On the other hand, the ^{13}C of pore water DIC decreases in the shallow part of the sediment down to $-60‰$, where sulfate diffused from seawater oxidizes methane, called anaerobic oxidation of methane (AOM). Despite the same ranges of $\delta^{13}C$ values, these systems differ greatly from the serpentinite-hosted vent systems. In case of the LCHF, the $\delta^{13}C$ values of carbonates varied from $-7‰$ to $+13‰$ [*Kelley et al*., 2005]. The ^{13}C-depleted values are closely related to the stable carbon isotope composition of the source fluid DIC ($\delta^{13}C = -8‰$ to $-2‰$) and the heavier shift of $\delta^{13}C$ values of carbonates would reflect the gradual precipitation from the residual DIC after ^{12}C-prefered biological consumption mainly by hydrogenotrophic methanogen [*Früh-Green et al*., 2003; *Kelley et al*., 2005]. Positive $\delta^{13}C$ values were also confirmed in some archaeal biomarkers, such as unsaturated pentamethylicosane derivatives (PMIs), squalenoids, sn-2 hydroxyarchaeol, and sn-3 hydroxyarchaeol, which were up to $+24.6‰$ [*Kelley et al*., 2005; *Bradley et al*., 2009; *Méhay et al*., 2013]. It has been explained that the ^{13}C-enriched biomarker can be attributed to near complete biological carbon consumption [*Bradley et al*., 2009; *Lang et al*., 2012; *Méhay et al*., 2013] under extremely low DIC concentration in the alkaline fluid (0.1–18 μM; <1000 to 10,000 lower than seawater DIC) [*Proskurowski et al*., 2006; *Schrenk et al*., 2013]. Similar endolithic microbial functions driven by the serpentinite fluid discharges may occur in SSF active (types I and II) chimneys. Although such microbial processes occur at the surface fraction of the active young chimneys in the LCHF, it could also occur at the inner porosities of the chimneys or subseafloor fluid conduit in the SSF because the higher $\delta^{13}C$ values occur in the inner parts of types I and II chimneys with lower porosity (~40% porosity). The reason why the maximum values of the $\delta^{13}C$ values of carbonates in the SSF chimneys reach $10‰$ above that in the LCHF is unknown because we could not collect pore or vent water from the SSF. In addition, the origin of a ^{13}C-depleted value ($\delta^{13}C = -8.8$) from type I chimney is also unknown, regarding whether this reflects the mantle-derived carbon or association of microbially produced ^{12}C-depleted carbon. Future investigations including vent water sampling trials, geochemical, microbiological, and organic chemical analysis will provide information explaining the higher and wide range of $\delta^{13}C$ in the carbonate in the SSF chimneys and allow us to better construct the carbon cycle in this new serpentinite-hosted vent system.

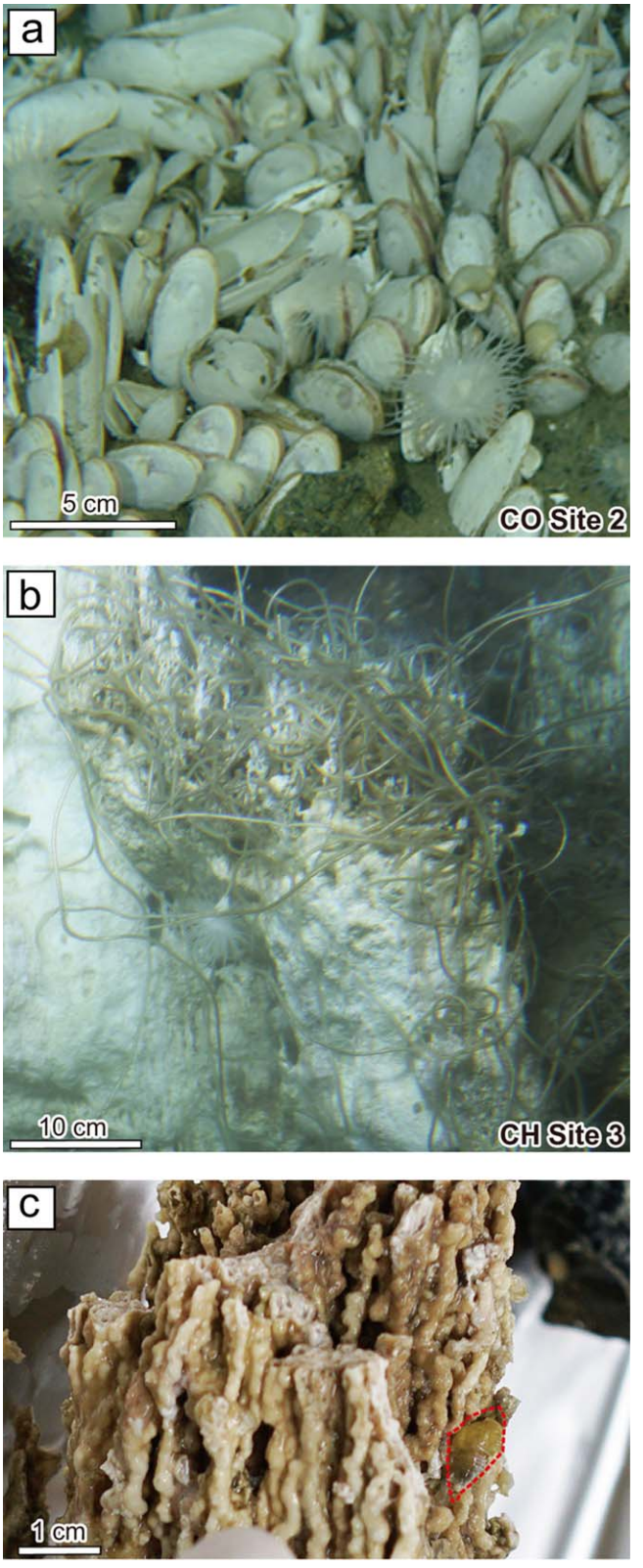

Figure 12. SSF macrofaunas. (a) Magnified view of a colony site (CO Site 2). Anthozoans and whelk *Bayerius* cf. *arnoldi* were observed with the large clam *Calyptogena* (*Abysogena*) *mariana*. (b) Magnified view of a type II chimney at CH Site3. *Phyllochaetopterus* sp. entangled on the chimney with anthozoans. (c) *Provanna* sp. (red dashed line) was only found inside the inner porous part of type II chimney.

Associated with the biogeochemical processes forming the chimney types described above, faunal communities on the different types of SSF chimneys also vary. Type I chimneys exhibited lower biomass dominated by microbial mats (Figure 4a), while the type II chimneys show higher biomass from the dense accumulation of a megafauna, the polychaete *Phyllocaetopterus* sp. (Figure 12b). The genus *Phyllocaetopterus* belongs to the family Chaetopteridae consisting of 12 genera, and is a filter-feeder inhabiting benthic chemosynthetic ecosystems [e.g., *Morineaux et al*., 2010; *Nishi and Rouse*, 2007, 2014]. One of the potential differences in the environmental conditions of the habitats associated with type I and type II chimneys could be the rate and amount of fluid supply—lower fluid discharge is expected at type II chimney sites compared to type I chimney sites. Perhaps the highly alkaline, Mg-rich fluid is less favorable for certain species. Less of this fluid may make type II chimney habitats more favorable for *Phyllocaetopterus* sp. In addition, the snail *Provanna* sp. has a very localized distribution, only occurring in the inner pores of type II chimneys at CH Site 3. *Provanna* species are generally deposit feeders, and the genus is endemic to chemosynthetic ecosystems (Chen et al., unpublished data). These observations suggest that the SSF system could support high-biomass, particularly in the chimneys and seafloor mineral deposits, even with reduced fluid supplies. Biomass observed in the SSF is higher than that around the LCHF. The scarcity of megafauna and the abundance of diverse meiofauna to macrofauna at the LCHF have been interpreted as characteristics for serpentinite-hosted systems in general, resulting from the fluid chemistry which is highly alkaline in pH, rich in CH_4 and H_2 but sulfide-poor [*Kelley et al*., 2005]. The

Table 6. Precipitation Rates of the Newly Grown Chimneys at CH Sites 3 and 4

	Details	CH Site3	CH Site4
(A) Estimated volume (cm^3)	From video images	250	1200
(B) Area of cutting edge (cm^2)	From video images	45	90
(C) Porosity	[a]	0.59	0.59
(D) Volume of solid fraction (cm^3)	A × C	102.5	492
(E) Volume of brucite (cm^3)	D × 0.9[b]	92.25	442.8
(F) Volume of $CaCO_3$ (cm^3)	D × 0.1[b]	10.25	49.2
(G) Brucite density (g/cm^3)		2.39	
(H) $CaCO_3$ density (g/cm^3)	[c]	2.77	
(I) Amount of brucite (g)	E × G	38.6	163.4
(I′) Amount of brucite (mol)	I ÷ 58.32	0.7	2.8
(J) Amount of $CaCO_3$ (g)	F × H	3.7	17.8
(J′) Amount of $CaCO_3$ (mol)	J ÷ 100.009	0.0	0.2
Brucite precipitation rate (mol cm^{-2} s^{-1})	I′ ÷ B ÷ 1 year[d]	4.7×10^{-10}	9.9×10^{-10}
$CaCO_3$ precipitation rate (mol cm^{-2} s^{-1})	J′ ÷ B ÷ 1 year[d]	2.6×10^{-11}	6.3×10^{-11}

[a]Maximum porosity of type I chimney, which was determined by area counting in thin section (details described in Method section).
[b]Based on the XRD analysis results, mineral composition of the newly grown chimney was set as brucite 90 wt % and $CaCO_3$ 10 wt %.
[c]Average value of calcite (2.71 g/cm^3) and aragonite densities (2.82 g/cm^3).
[d]One year in s = 365 × 24 × 60 × 60.

LCHF community is very different from black smoker hydrothermal vent communities, which are characterized by dense megafaunal populations [e.g., *Van Dover*, 2000]. However, a fossil example showing high-biomass chemosynthetic community at a serpentinite-hosted system has been reported [*Lartaud et al*., 2011]. This is the Ghost City site on the MAR, near the Rainbow hydrothermal field, where LCHF-type carbonates contain a variety of fossils including chemosynthetic mussels and clams with associated gastropods [*Lartaud et al*., 2011]. Clearly we have much to learn about communities associated with seafloor serpentine-hosted hydrothermal and seep systems. Further ecological and biological investigations in the SSF promise to lead to a new understanding of chemosynthetic ecosystems supported by the serpentinite fluid discharges.

Collectively, this study suggests that the morphological and mineralogical variations of the SSF chimneys are subject to a balance between precipitation and dissolution processes, and the transition between these processes. Figures 13a and 13b summarizes the characteristics of the three chimney types in the SSF and compares SSF and LCHF chimneys [*Ludwig et al*., 2006], respectively. Especially, the brucite-dominated (up to 99 wt %) type I chimney and the porous structure (∼50%) of type III chimney are unique to the SSF. These unique characteristics likely result from venting conditions of cold fluid and mixing with

Table 7. Estimated Dissolution Rates of the Whole Chimney Structure Discovered in the SSF Under Some Assumption

	Details	Value	Unit
(A) Volume of total chimney structure	From video images	12.4	m^3
(B) Porosity	Average value	50	%
(C) Volume of solid fraction	A × C	6.2	m^3
(D) Content ratio of brucite	Average value	60	%
(E) Content ratio of $CaCO_3$	Average value	40	%
(E) Volume of brucite	C × D × 10^6	3.7×10^6	cm^3
(F) Volume of $CaCO_3$	C × E × 10^6	2.5×10^6	cm^3
(G) Surficial area of brucite cuboid	From x^3 = E, $x^2 \times 6$ = G	1.4×10^5	cm^2
(H) Surficial area of $CaCO_3$ cuboid	From x^3 = F, $x^2 \times 6$ = H	1.1×10^5	cm^2
(I) Bumpy surficial area of brucite cuboid	G × 7755[a]	1.1×10^9	cm^2
(J) Bumpy surficial area of $CaCO_3$ cuboid	H × 6775[a]	7.5×10^9	cm^2
(K) Brucite amount	2.39 × E/58.32**	12.5×10^4	mol
(L) $CaCO_3$ amount	2.77 × E/100.009**	5.6×10^4	mol
(M) Brucite dissolution rates	Refs. 1 and 2	$0.5–1.0 \times 10^{-12}$	mol cm^{-2} s^{-1}
(N) $CaCO_3$ dissolution rates	Refs. 4 and 5	$0.7–5.4 \times 10^{-13}$	mol cm^{-2} s^{-1}
(O) Time for brucite dissolve away	((K/I)/M)/(60 × 60 × 24 × 365)	3.6–7.3	year
(P) Time for $CaCO_3$ dissolve away	((LJI)/N)/(60 × 60 × 24 × 365)	4.4–34.3	year

[a]Increasing ratio of the surficial area in case of the cuboid made by 100 μm cubic crystals. **Used same values of density listed in Table 6.
Refs. (1) *Pokrovsky and Schott* [2004], (2) *Kudoh et al*. [2006], (3) *Peterson* [1966], (4) *Milliman* [1977], (5) *Berelson et al*. [1990].

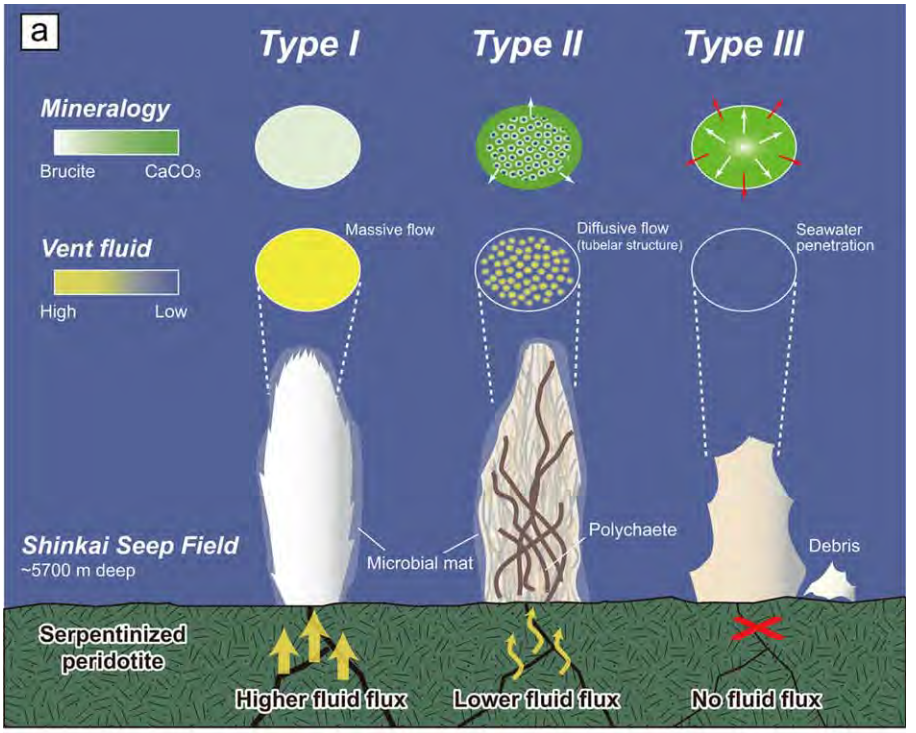

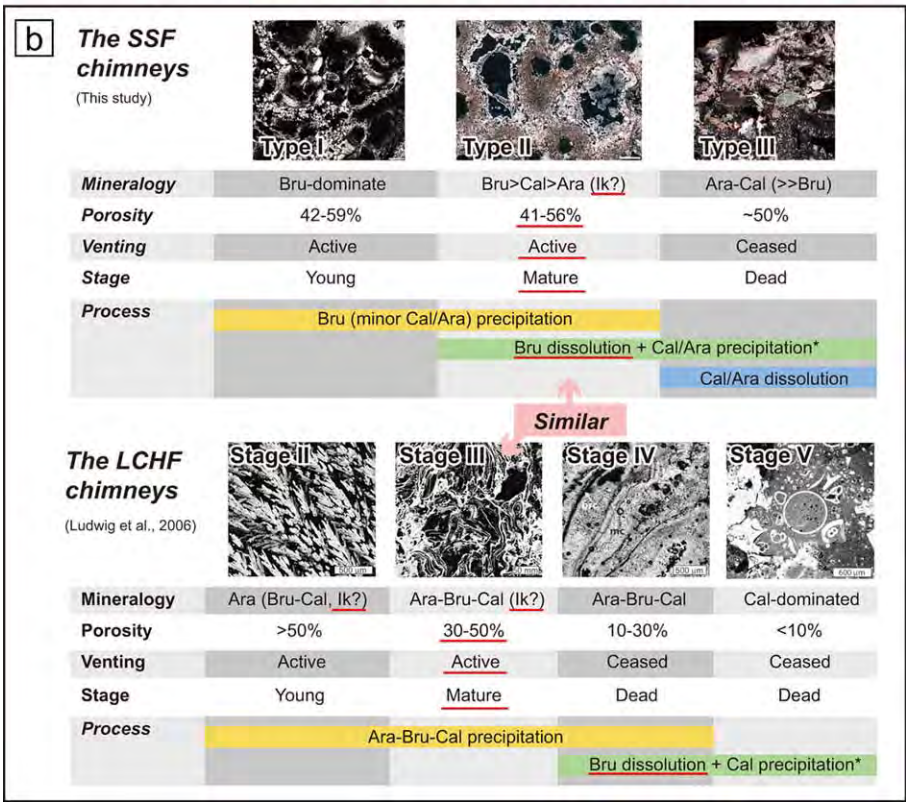

Figure 13. Illustration summarizing characteristics of the three types (I–III) of SSF chimneys. (a) The ellipses are frame format of the chimney cross sections showing mineralogy (top) and assumed fluid-seawater mixing ratio (bottom). $CaCO_3$ in outer layers of type II chimney and most of type III chimney is considered to be secondary precipitation induced by brucite dissolution (white arrows). The outer carbonate layer of type III chimneys is also dissolving (red arrows) and formed surface depressions like karren (denudation of karst). (b) Textures and formation settings of the SSF chimneys, in comparison with the LCHF chimneys. Results of the LCHF chimneys are compiled from *Ludwig et al*. [2006]. Photographs showing the microtexture of the LCHF chimneys are taken from Figure 4 in *Ludwig et al*. [2006, p. 3633]. See discussion section for details.

undersaturated ambient seawater at greater depth. On the other hand, existing ikaite crystals, sinuous tubular structures, and development of bushy-mushroom microbial mat are commonly observed in types I–II SSF chimneys and stage III of the LCHF chimney (Figure 13b). The common characteristics result from similar mechanisms that occur in the SSF and the LCHF.

Brucite-carbonate chimneys in an active serpentinization system have been reported from the Cerulean Springs at Pacman Seamount in northern Mariana Forearc [*Fryer et al*., 1999], the LCHF [e.g., *Kelley et al*., 2001], and Prony Bay, New Caledonia [e.g., *Monnin et al*., 2014]. Detailed geochemical and sedimentological processes for chimney formation, however, have been reported only from the LCHF [*Ludwig et al*., 2006]. Therefore, the LCHF chimneys have been the only example for interpreting inferred carbonates associated with serpentinite, such as Ordovician carbonate in the Canadian Appalachians [*Lavoie and Chi*, 2010] and Cretaceous carbonate at the Iberia Margin [*Schwarzenbach et al*., 2013; *Klein et al*., 2015]. Discovery and description of the SSF chimneys uncovered unknown variability in the sedimentological, mineralogical, and isotopic features of precipitates at serpentinite-hosted vent systems, and as such our present results provide new insight for interpreting such geological samples. Moreover, seeping activities estimated from the chimney appearances will provide useful information for understanding the geology at the southern Mariana forearc, which is still controversial [*Stern et al*., 2014].

6 Conclusions

We studied chimneys and ecosystems at the Shinkai Seep Field (SSF) in the southern Mariana forearc, the deepest known serpentinite-hosted system in the world. The following conclusions can be drawn based on the observations and interpretations presented in this paper:

1. The SSF includes 11 vesicomyid clam colony sites and four chimney sites, distributed within a ~500 m square area centered at 11°39.36′N, 143°02.86′E.
2. SSF chimney sites occur at around 5700 m depth, on exposed bedrocks of serpentinized peridotite, well below the CCD. This is the deepest known serpentinite-hosted vent field. Formation of carbonate chimneys below the CCD is demonstrated.
3. SSF chimneys consisted of brucite, calcite, and aragonite in variable proportions. Rare possible ikaite is recognized in type II chimneys, perhaps representing a transitional phase in the conversion of brucite to carbonate.
4. From chimney appearances, microtextures, and faunal communities, the SSF chimneys can be categorized into three types:
   A. Type I chimneys are made of brucite. Their outer surfaces are bright white to light yellow colored with spiky crystalline and wrinkled surface texture. These are covered by bushy or mushroom-shaped white microbial mat. This type is considered as the active structure precipitated under high fluid discharge conditions. The fluid must be high-pH in order to precipitate brucite.
   B. Type II chimneys are zoned, brucite on the inside and carbonate (calcite or aragonite) on the outside. The outer surfaces of type II chimneys are white to dull brown colored with tuberous textures like vascular bundles. These exhibit grayish microbial mat with dense accumulations of *Phyllochaetopterus* sp. This type is considered as an active structure precipitated from lower fluid discharging condition.
   C. Type III chimneys are made of carbonate. These are ivory colored with smooth surface and depressions like karren (denudation of karst). These lack living microbial mat or animals. They are relict structures with all brucite replaced by carbonate.
5. Carbon isotope values of type I and inner part of type II chimneys show a wide range from −8.8 to +24.1‰. Enrichment of ^{13}C likely reflects biological ^{12}C consumption occurring within extremely carbon-limited fluid. In contrast, type III and outer parts of type II chimneys have near seawater DIC values (~0‰).
6. Faunal communities on type II chimneys indicate that high biomass could occur on chimneys of a serpentinite-hosted vent systems.

Finding the SSF chimneys showed that serpentinite-hosted seep system can occur not only along mid-oceanic ridges and forearc seamounts as previously known, but also on forearc slopes where peridotite is exposed. In addition, faunal communities on these chimneys demonstrated that serpentinite-hosted

systems are capable of hosting high-biomass ecosystems. Future studies of the SSF will enhance our knowledge and understanding of seafloor serpentinite-hosted hydrothermal systems and their communities. This is especially significant because serpentinization is likely to have happened throughout the Earth's history, and is also thought to occur on other planets where water and ultramafic rocks might be present.

Acknowledgments

The authors would thank the *Shinkai* 6500 operation team and the crew of the R/V *Yokosuka* for their professional support during the YK10-08, YK13-08, YK14-13, and YK15-11 Cruise. This study was conducted under the special permit of US Fish and Wildlife Service for studies in the Mariana Trench Marine National Monument. On-board samplings and discussions were performed under the support of the scientific parties of the cruises as listed below; Osamu Ishizuka, Uta Konno, Genki Ozawa, Masakazu Fujii, Masashi Ito, Fernando Martinez, Maryjo Brounce, Yusuke Miyajima, Shoma Oya, Tomoki Mizuno, Takuro Nunoura, Akinori Yabuki, and Miho Hirai. We also gratefully acknowledge Shinsuke Kawagucci and Akihiro Kano for their constructive discussions. Some thin sections were outsourced to Hokushin Koki Factory, Tokyo, Japan. Minoru Ikehara supported a part of stable carbon isotope analysis. We thank two anonymous reviewers for providing constructive comments. This project was partly founded by the Ministry of Education, Culture, Sports, Science, and Technology, Japan, by a grant-in-aids for Young Scientists (15H05468) and a JSPS research fellowship for young scientist (26-10363) to TO. Participation of US scientists was made possible by NSF grants EAR 0840862 and 1026150. The authors have no conflict of interests to declare. A video is provided as supporting information to show appearances of the chimneys at SSF. The data used are listed in the references, tables, figures and supporting information. The cruises information is provided by the Japan Agency for Marine-Earth Science and Technology (JAMSTEC) and available via the JAMSTEC data website (http://www.godac.jamstec.go.jp/darwin/e/).

References

Berelson, W. M., D. E. Hammond, and G. A. Cutter (1990), In situ measurements of calcium carbonate dissolution rates in deep-sea sediments, *Geohim. Cosmohim. Acta*, *54*, 3013–3020.

Bradley, A. S., and R. E. Summons (2010), Multiple origins of methane at the Lost City Hydrothermal Field, *Earth Planet. Sci. Lett.*, *297*, 34–41.

Bradley, A. S., J. M. Hayes, and R. E. Summons (2009), Extraordinary ^{13}C enrichment of diether lipids at the Lost City Hydrothermal Field indicates a carbon-limited ecosystem, *Geochim. Cosmochim. Acta*, *73*, 102–118, doi:10.1016/j.gca.2008.10.005

Brazelton, W. J., M. O. Schrenk, D. S. Kelley, and J. A. Baross (2006), Methane- and sulfur-metabolizing microbial communities dominate the Lost City Hydrothermal Field Ecosystem, *Appl. Environ. Microbiol.*, *72*, 6257–6270.

Buchardt, B., et al. (1997), Submarine columns of ikaite tufa, *Nature*, *390*, 239–130.

Charlou, J. L., J. P. Donval, P. Jean-Baptiste, and N. Holm (2002), Geochemistry of high H_2 and CH_4 vent fluid issuing from ultramafic rocks at the Rainbow hydrothermal field (36°14′N, MAR), *Chem. Geol.*, *191*, 345–359, doi:10.1016/S0009-2541(02)00134-1.

Chatterjee, S., G. R. Dickens, G. Bhatnagar, W. G. Chapman, B. Dugan, G. T. Snyder, and G. J. Hirasaki (2011), Pore water sulfate, alkalinity, and carbon isotope profiles in shallow sediment above marine gas hydrate systems: A numerical modeling perspective, *J. Geophys. Res.*, *116*, B09103, doi:10.1029/2011JB008290.

Craig, H. (1957), Isotopic standards for carbon and oxygen and correction factors for mass-spectrometric analysis of carbon dioxide, *Geochim. Cosmochim. Acta*, *12*, 133–149.

DeChaine, E. G., A. E. Bates, T. M. Shank, and C. M. Cavanaugh (2006), Off-axis symbiosis found: Characterization and biogeography of bacterial symbionts of *Bathymodiolus* mussels from Lost City hydrothermal vents, *Environ. Microbiol.*, *8*, 1902–1912, doi:10.1111/j.1462-2920.2005.01113.x.

Folk, R. L. (1974), The natural history of crystalline calcium carbonate: Effect of magnesium content and salinity, *J. Sediment. Petrol.*, *44*, 40–53.

Folk, R. L. (1994), Interaction between bacteria, nannobacteria and mineral precipitation in hot springs of central Italy, *Géogr. Phys. Quat.*, *48*, 233–46.

Früh-Green, G. L., D. S. Kelley, S. M. Barnasconi, J. A. Karson, K. A. Ludwig, D. Butterfield, C. Boschi, and G. Proskurowski (2003), 30,000 years of hydrothermal activity at the Lost City vent field, *Science*, *301*, 495–498, doi:10.1126/science.1085582.

Fryer, P. (1996), Evolution of the Mariana convergent plate margin system, *Rev. Geophys.*, *34*, 89–126.

Fryer, P. (2003), Serpentinite mud volcanism: Observations, processes and implications, *Annu. Rev. Mar. Sci.*, *4*, 345–373.

Fryer, P., C. G. Wheat, and M. L. Mottl (1999), Mariana blueschist mud volcanism: Implications for conditions within the subduction zone, *Geology*, *27*, 103–106.

Gieskes, J. M., T. Gamo, and H. Brumsack (1991), Chemical methods for interstitial water analysis aboard Joides Resolution. In *ODP Technical Note*, No. 15, 60 pp.

Greinert, J., G. Bohrmann, and E. Suess (2001), Gas hydrate associated carbonates and methane-venting at Hydrate Ridge: Classification, distribution and origin of authigenic lithologies, in *Natural Gas Hydrates: Occurrence, Distribution, and Detection*, edited by C. K. Paull and W.P. Dillon, pp. 99–113, AGU, Washington, D. C.

Gvirtzman, Z., and R. J., Stern (2004), Bathymetry of Mariana Trench-Arc system and formation of the challenger deep as a consequence of weak plate coupling, *Tectonics*, *23*, TC2011, doi:10.1029/2003TC001581.

Haggerty, J. A. (1991), Evidence from fluid seeps atop serpentine seamounts in the Mariana forearc: Clues for emplacement of the seamounts and their relationship to forearc tectonics, *Mar. Geol.*, *201*, 293–309, doi:10.1016/0025-3227(91)90013-T.

Hannington, M. D., I. R. Jonasson, P. M. Herzig, and S. Peterson (1995), Physical and chemical processes of seafloor mineralization at mid-ocean ridges, in *Seafloor Hydrothermal Systems: Physical, Chemical, Biological and Geological Interactions*, edited by S. E. Humphiris, et al., vol. 91, pp. 115–157, AGU, Washington, D. C.

Heuer, V. B., J. W. Pohlman, M. E. Torres, M. Elvert, and K.-U. Hinrichs (2009), The stable carbon isotope biogeochemistry of acetate and other dissolved carbon species in deep subseafloor sediments at the northern Cascadia Margin, *Geohim. Cosmohim. Acta*, *73*, 3323–3336. doi:10.1016/j.gca.2009.03.001.

Hu, Y.-B., D. A. Wolf-Gladrow, S. G. Dieckmann, C. Völker, and G. Nehrrke (2014), A laboratory study of ikaite ($CaCO_3{\cdot}6H_2O$) precipitation as a function of pH, salinity, temperature and phosphate concentration, *Mar. Chem.*, *162*, 10–18, doi:10.1016/j.marchem.2014.02.003.

Kato, K., H. Wada, and K. Fujioka (1998), Carbon and oxygen isotope composition of carbonate chimney from Mariana forearc seamount, *JAMSTEC Deep Sea Res.*, *14*, 213–222.

Kelley, D. S., et al. (2001), An off-axis hydrothermal vent field near the Mid-Atlantic Ridge at 30°N, *Nature*, *412*, 145–149.

Kelley, D. S., et al. (2005), A serpentinite-hosted ecosystem: The Lost City Hydrothermal Field, *Science*, *307*, 1428–1434, doi:10.1126/science.1102556.

Kinsey, J. C. and C. R. German (2013), Sustained volcanically-hosted venting at ultraslow ridges: Piccard Hydrothermal Field, *Mid-Cayman Rise. Earth Planet. Sci. Lett.*, 380, 162–168.

Klein, F., S. E. Humphris, W. Guo, F. Schubotz, E. M. Schwarzenback, and W. D. Orsi (2015), Fluid mixing and the deep biosphere of a fossil Lost City-type hydrothermal system at the Iberia Margin, *Proc. Natl. Acad. Sci. U. S. A.*, *112*, 12,036–12,041, doi:10.1073/pnas.1504674112.

Kontoyannis, C. G., M. G. Orkoula, and P. G. Koutsoukos (1997), Quantitative analysis of sulfated calcium carbonates using Raman spectroscopy and X-ray powder diffraction, *Analyst*, *122*, 38–37.

Lang, S. Q., G. L. Früg-Green, S. M. Berbasconi, M. D. Lilley, G. Proskurowski, S. Méhay, and D. A. Butterfield (2012), Microbial utilizeation of abiogenic carbon and hydrogen in a serpentinite-hosted system, *Geohim. Cosmohim. Acta*, *92*, 82–99, doi:10.1016/j.gca.2012.06.006.

Lartaud, F., C. T. S. Little, M. De Rafelis, G. Bayon, J. Dyment, B. Ildefonse, V. Gressier, Y. Fouquet, F. Gaill, and N. Le Bris (2011), Fossil evidence for serpentinization fluids fueling chemosynthetic assemblages, *Proc. Natl. Acad. Sci. U. S. A.*, *108*, 7698–7703, doi:10.1073/pnas.1009383108.

Launay, J., and J. C. Fontes (1985), Les sources thermales de Prony (Nouvelle Calédonie) et leurs précipités chimiques, exemple de formation de brucite primaire, *Geol. France*, *1*, 83–100.

Lavoie, D., and G. Chi (2010), An Ordovician "Lost City"-venting serpentinite and like oases on lappets seafloor, *Can. J. Earth Sci.*, *47*, 199–207.
López-García, P., A. Vereshchaka, and D. Moreira (2007), Eukayotic diversity associated with carbonates and fluid-seawater interface in Lost City hydrothermal field, *Environ. Microbiol.*, *9*, 546–554, doi:10.1111/j.1462-2920.2006.01158.x.
Ludwig, K. A., D. S. Kelley, D. A. Butterfield, B. K. Nelson, and G. L. Früh-Green (2006), Formation and evolution of carbonate chimneys at the Lost City Hydrothermal Field, *Geochim. Cosmochim. Acta*, *70*, 3625–3645.
Martin, W., J. Baross, D. Kelley, and M. J. Russell (2008), Hydrothermal vents and the origin of life, *Nat. Rev. Microbiol.*, *6*, 805–814, doi:10.1038/nrmicro1991.
McCollom, T. M. (2013), Laboratory simulations of abiotic hydrocarbon formation in earth deep subsurface, *Rev. Mineral. Geochem.*, *75*, 467–494.
McCollom, T. M., and J. S. Seewald (2001), A reassessment of the potential for reduction of dissolved CO_2 to hydrocarbons during serpentinization of olivine, *Geochim. Cosmochim. Acta*, *65*, 3769–3778.
McCollom, T. M., and W. Bach (2009), Thermodynamic constraints on hydrogen generation during serpentinization of ultramafic rocks, *Geochim. Cosmochim. Acta*, *73*, 856–875.
Méhay, S., G. L. Früg-Green, S. Q. Lang, S. M. Bernasconi, W. J. Brazelton, M. O. Schrenk, P. Schaeffer, and P. Adam (2013), Record of archaeal activity at the serpentinite-hosted Lost City Hydrothermal Field, *Geobiology*, *11*, 570–592, doi:10.1111/gbi.12062.
Monnin, C., et al. (2014), Fluid chemistry of the low temperature hyperalkaline hydrothermal system of Prony Bay (New Caledonia), *Biogeosciences*, *11*, 5687–5706.***
Milliman, J. D. (1977) Dissolution of calcium carbonate in the Sargasso Sea (northwest Atlantic), in *Fate of Fossil CO2 in the Oceans*, edited by N. Anderson and A. Manahof, pp. 641–653, Plenum Press, N. Y.
Morineaux, M., E. Nishi, A. Ormos, and O. Mouchel (2010), A new species of *Phyllochaetopterus* (Annelida: Chaetopteridae) from deep-sea hydrothermal Ashadze-1 vent field, Mid-Atlantic Ridge: Taxonomical description and partial COI DNA sequence, *Cah. Biol. Mar.*, *51*, 239–248.
Murray, J. W. (1954), The deposition of calcite and aragonite in caves, *J. Geol.*, *62*, 481–492.
Naehr, T. H., P. Eichhubl, V. J. Orphan, M. Hovland, C. K. Paull, W. Ussler III, T. D. Lorenson, and H. G. Greene (2007), Authigenic carbonate formation at hydrocarbon seeps in continental margin sediments: A comparative study, *Deep sea Res., Part I*, *54*, 1268–1291, doi:10.1016/j.dsr2.2007.04.010.
Nakamura, K., and K. Takai (2014), Theoretical constraints of physical and chemical properties of hydrothermal fluids on variations in chemolithotrophic microbial communities in seafloor hydrothermal systems, *Prog. Earth Planet. Sci.*, *1*, 5, doi:10.1186/2197-4284-1-5.
Nakamura, K., T. Morishita, W. Bach, F. Klein, K. Hara, K. Okino, K. Takai, and H. Kumagai (2009), Serpentinized troctolites exposed near the Kairei Hydrothermal Field, Central Indian Ridge: Insights into the origin of the Kairei hydrothermal fluid supporting a unique microbial ecosystem, *Earth Planet. Sci. Rev.*, *280*, 128–136.
Nishi, E., and G. Rouse (2007), A new species of *Phyllochaetopterus* (Chaetopteridae: Annelida) from near hydrothermal vents in the Lau Basin, western Pacific Ocean, *Zootaxa*, *1621*, 55–64.
Nishi, E., and G. Rouse (2014), First whale fall chaetopterid: A gigantic new species of *Phyllochaetopterus* (Chaetopteridae: Annelida) from the deep sea off California, *Proc. Biol. Soc. Wash.*, *126*, 287–298.
Ohara, Y., et al. (2012), A serpentinite-hosted ecosystem in the Southern Mariana Forearc, *Proc. Natl. Acad. Sci. U. S. A.*, *109*, 2831–2835, doi:10.1073/pnas.1112005109.
Okutani, T., K. Fujikura, H. Watanabe, and Y. Ohara (2013), *Calyptogena* (*Abyssogena*) mariana: Discovery of a new vesicomyid clam from the Mariana Trench, *Venus*, *71*, 39–47.
Orphan, V. J., W. Ussler, T. H. Naehr, C. H. House, K.-U. Hinrichs, and C. K. Paull (2004), Geological, geochemical, and microbiological heterogeneity of the seafloor around methane vents in the Eel River Basin, offshore California, *Chem. Geol.*, *205*, 265–289, doi:10.1016/j.chemgeo.2003.12.035.
Palandri, J. L., and M. H. Reed (2004), Geochemical models of metasomatism in ultramafic systems: Serpentinization, rodingitization, and sea floor carbonate chimney precipitation, *Geochim. Cosmochim. Acta*, *68*, 2226–1133.
Parkhurst, D. L., and C. A. J. Appelo (2013), Description of input and examples for PHREEQC version 3—A computer program for speciation, batch-reaction, one-dimensional transport, and inverse geochemical calculations, in *U.S. Geological Survey Techniques and Methods*, Book 6, chap. A43, 497 pp., USGS, VA, USA. [Available at http://pubs.usgs.gov/tm/06/a43/.]
Peterson, M. N. A. (1966), Calcite: Rates of dissolution in a vertical profile in the central Pacific, *Science*, *154*, 1542–1544.
Pokrovsky, O. S., and J. Schott (2004), Experimental study of brucite dissolution and precipitation in aqueous solutions: Surface speciation and chemical affinity control, *Geochim. Cosmohim. Acta*, *68*, 31–45, doi:10.1016/S0016-7037(03)00238-2.
Proskurowski, G., M. D. Lilley, D. S. Kelley, and E. J. Olson (2006), Low temperature volatile production at the Lost City Hydrothermal field, evidence from a hydrogen stable isotope geothermometer, *Chem. Geol.*, *229*, 331–343, doi:10.1016/j.chemgeo.2005.11.005.
Proskurowski, G., M. D. Lilley, J. S. Seewald, G. L. Früh-Green, E. J. Olson, J. E. Lupton, S. P. Sylva, and D. S. Kelley (2008), Abiogenic hydrocarbon production at Lost City Hydrothermal Field, *Science*, *319*, 604–607, doi:10.1126/science.1151194.
Rasumussen, B. (2000), Filamentous microfossils in a 3,235-million-year-old volcanogenic massive sulphide deposit, *Nature*, *504*, 676–679.
Ribeiro, J. M., et al. (2013), Geodynamic evolution of a forearc rift in the southernmost Mariana Arc, *Island Arc*, *22*, 453–476.
Rickaby, R. E. M., S. Shaw, G. Bennitt, H. Kennedy, M. Zabel, and A. Lennie (2006), Potential of ikaite to record the evolution of oceanic $\delta^{18}O$, *Geology*, *34*, 497–500, doi:10.1130/G22413.1.
Sample, J. C., and A. Kopf (1995), Isotope geochemistry of syntectonic carbonate cements and veins from the Oregon Margin: Implications for the hydrogeologic evolution of the accretion wedge, *Proc. Ocean Dlill. Prog. Sci. Results*, *146*, 137–148.
Schrenk, M. O., D. S. Kelley, S. A. Bolton, and J. A. Baross (2004), Low archaeal diversity linked to subseafloor geochemical processes at the Lost City Hydrothermal Field, Mid-Atlantic Ridge, *Environ. Microbiol.*, *6*, 1086–1095, doi:10.1111/j.1462-2920.2004.00650.x.
Schrenk, M.O., W. J. Brazelton, and S. Q. Lang (2013), Serpentinization, carbon, and deep life, *Rev. Mineral. Gheochem.*, *75*, 575–606.
Schwarzenbach, E. M., G. L. Früh-Green, S. M. Bernasconi, J. C. Alt, and A. Plas (2013), Serpentinization and carbon sequestration: A study of two ancient peridotite-hosted hydrothermal systems, *Chem. Geol.*, *351*, 115–133, doi:10.1016/j.chemgeo.2013.05.016.
Seibold, E., and W. H. Berger (1996), *The Sea Floor: An Introduction to Marine Geology*, 356 pp., Springer, Berlin.
Seyfried, W. E., Jr., N. J. Pester, B. M. Tutolo, and K. Ding (2015), The Lost City hydrothermal system: Constraints imposed by vent fluid chemistry and reaction path models on subseafloor heat and mass transfer processes, *Geochim. Cosmochim. Acta*, *163*, 59–79, doi:10.1016/i.gca.2015.04.040.
Sleep, N. H., A. Meibom, T. H. Fridriksson, R. G. Coleman, and D. K. Bird (2004), H_2-rich fluids from serpentinization: Geochemical and biotic implications, *Proc. Natl. Acad. Sci. U. S. A.*, *101*, 12,818–12,823, doi:10.1073/pnas.0405289101.

Stern R. J., and N. C. Smoot (1998), A bathymetric overview of the Mariana forearc, *Island Arc*, *7*, 525–540.
Stern, R. J., Y. Tamura, H. Masuda, P. Fryer, F. Martinez, O. Ishizuka, and S. H. Bloomer (2013), How does the Mariana Arc end in the south?, *Island Arc*, *22*, 133–148.
Stern, R. J., M. Ren, K. A. Kelley, Y. Ohara, F. Martinez, and S. H. Bloomer (2014), Basaltic volcaniclastics from the Challenger Deep forearc segment, Mariana convergent margin: Implications for tectonics and magmatism of the southernmost Izu-Bonin-Mariana arc, *Island Arc*, *23*, 368–382. doi:10.1111/iar.12088.
Ueno, Y., Y. Isozaki, H. Yurimoto, and S. Maruyama (2001), Carbon isotopic signatures of individual, Archean, probable microfossils from Western Australia, *Int. Geol. Rev.*, *43*, 196–212.
Ueno, Y., H. Yoshioka, S. Maruyama, and Y. Isozaki (2004), Carbon isotopes and petrograph of kerogens in 3.5-Ga hydrothermal silica dikes in the North Pole area, Western Australia, *Geochim. Cosmohim. Acta*, *68*, 573–589.
Ueno, Y., K. Yamada, N. Yoshida, S. Maruyama, and Y. Isozaki (2006), Evidence from fluid inclusions fro microbial methanogenesis in the early Archean era. *Nature*, *440*, 516–519.
Yamanaka, T., C. Mizota, H. Satake, F. Kouzuma, T. Gamo, U. Tsunogai, T. Miwa, and K. Fujioka (2003), Stable isotope evidence for a putative endosymbiont-based lithotrophic *Bathymodiolus* sp. mussel community atop a serpentine seamount, *Geomicrobiol. J.*, *20*, 185–197.
Van Dover, C. L. (2000), *The Ecology of Deep-Sea Hydrothermal Vents*, 424 pp., Princeton Univ. Press, Princeton, N. J.
Webber, A. P, S. Roberts, B. J. Murton, and M. R. S. Hodgkinson (2015), Geology, sulphide geochemistry and supercritical venting at the Beebe Hydrothermal Vent Field, Cayman Trough. *Geochem. Geophys. Geosyst*. doi:10.1002/2015GC005879.
Wheat, C. G., P. Fryer, K. Takai, and S. Hulme (2010), Spotlight 9: South Chamorro Seamount, *Oceanography*, *23*, 174–175.
Woese, C. R., and G. E. Fox (1977), Phylogenetic structure of the prokaryotic domain: The primary kingdoms, *Proc. Natl. Acad. Sci. U. S. A.*, *74*, 5088–5090.